TECHNICAL REPORT RD-CR-85-9

NUMERICAL SIMULATION OF AXISYMMETRIC BASE FLOW ON TACTICAL MISSILES WITH PROPULSIVE JET

P.D. Thomas, R.P. Reklis,
R.R. Roloff, and R.J. Conti
Lockheed Palo Alto Research Laboratory
Lockheed Missiles & Space Co., Inc.
3251 Hanover Street
Palo Alto, CA 94304

NOVEMBER 1987

Prepared for:
System Simulation and Development Directorate
Research, Development, and Engineering Center

Contract No. DAAH01-82-C-0519

U.S. ARMY MISSILE COMMAND
Redstone Arsenal, Alabama 35898-5000

Approved for public release; distribution is unlimited.

DISPOSITION INSTRUCTIONS

DESTROY THIS REPORT WHEN IT IS NO LONGER NEEDED. DO NOT RETURN IT TO THE ORIGINATOR.

DISCLAIMER

THE FINDINGS IN THIS REPORT ARE NOT TO BE CONSTRUED AS AN OFFICIAL DEPARTMENT OF THE ARMY POSITION UNLESS SO DESIGNATED BY OTHER AUTHORIZED DOCUMENTS.

TRADE NAMES

USE OF TRADE NAMES OR MANUFACTURERS IN THIS REPORT DOES NOT CONSTITUTE AN OFFICIAL INDORSEMENT OR APPROVAL OF THE USE OF SUCH COMMERCIAL HARDWARE OR SOFTWARE.

UNCLASSIFIED
SECURITY CLASSIFICATION OF THIS PAGE

AD-A196 169

REPORT DOCUMENTATION PAGE

Form Approved
OMB No. 0704-0188
Exp. Date: Jun 30, 1986

1a. REPORT SECURITY CLASSIFICATION Unclassified	1b. RESTRICTIVE MARKINGS
2a. SECURITY CLASSIFICATION AUTHORITY	3. DISTRIBUTION/AVAILABILITY OF REPORT Cleared for public release; distribution is unlimited
2b. DECLASSIFICATION/DOWNGRADING SCHEDULE	
4. PERFORMING ORGANIZATION REPORT NUMBER(S) LMSC-D878344	5. MONITORING ORGANIZATION REPORT NUMBER(S) RD-CR-85-9
6a. NAME OF PERFORMING ORGANIZATION Lockheed Missiles and Space Co., Inc.	6b. OFFICE SYMBOL (If applicable)
6c. ADDRESS (City, State, and ZIP Code) 3251 Hanover St. Palo Alto, CA 94304	7a. NAME OF MONITORING ORGANIZATION 7b. ADDRESS (City, State, and ZIP Code)
8a. NAME OF FUNDING/SPONSORING ORGANIZATION Sys Sim and Dev Dir	8b. OFFICE SYMBOL (If applicable) AMSMI-RD-SS-AT
8c. ADDRESS (City, State, and ZIP Code) Commander, U.S. Army Missile Command ATTN: AMSMI-RD-SS-AT Redstone Arsenal, AL 35898-5252	9. PROCUREMENT INSTRUMENT IDENTIFICATION NUMBER 10. SOURCE OF FUNDING NUMBERS

PROGRAM ELEMENT NO.	PROJECT NO.	TASK NO.	WORK UNIT ACCESSION NO

11. TITLE (Include Security Classification)
Numerical Simulation of Axisymmetric Base Flow on Tactical Missiles with Propulsive Jet

12. PERSONAL AUTHOR(S)
P.D. Thomas, R.P. Reklis, R.R. Roloff, and R.J. Conti

13a. TYPE OF REPORT	13b. TIME COVERED	14. DATE OF REPORT (Year, Month, Day)	15. PAGE COUNT
Final	FROM Jul 82 TO Aug 83	NOVEMBER 1987	44

16. SUPPLEMENTARY NOTATION

17. COSATI CODES		
FIELD	GROUP	SUB-GROUP

18. SUBJECT TERMS (Continue on reverse if necessary and identify by block number)
Base flow
Tactical missiles
Navier-Stokes
Near wake

19. ABSTRACT (Continue on reverse if necessary and identify by block number)

The axisymmetric Lockheed Viscous Implicit Solver (LVIS) Navier-Stokes computer code is modified to incorporate the capability for computing the flow in the base region of a tactical missile with propulsive jet. Modifications include generalization of the computational space to accomodate the geometry of the base and implementation of two turbulence models of the two-equation type (k-epsilon and k-W). Computer runs are made with both turbulence models. The results of these computations are similar, but some differences are observed in the recirculating near-wake flow and in the shear layers that separate it from the high-speed streams of the propulsive jet and of the external flow. These differences are attributed to the greater eddy viscosity predicted by the k-epsilon model.

20. DISTRIBUTION/AVAILABILITY OF ABSTRACT	21. ABSTRACT SECURITY CLASSIFICATION
☒ UNCLASSIFIED/UNLIMITED ☐ SAME AS RPT. ☐ DTIC USERS	Unclassified

22a. NAME OF RESPONSIBLE INDIVIDUAL	22b TELEPHONE (Include Area Code)	22c. OFFICE SYMBOL
Billy J. Walker	(205) 876-7278	AMSMI-RD-SS-AT

DD FORM 1473, 84 MAR — 83 APR edition may be used until exhausted. All other editions are obsolete.

SECURITY CLASSIFICATION OF THIS PAGE
UNCLASSIFIED

TABLE OF CONTENTS

LIST OF ILLUSTRATIONS

LIST OF ILLUSTRATIONS (CONTINUED)

1. INTRODUCTION

This report describes the work performed under Contract DAAH01-82-C-0519, "Tactical Missile Base Flow," which addresses Task II of Technical Requirement 0119, of October 21, 1980. The purpose of the Task II effort is to investigate the feasibility of applying advanced Navier-Stokes numerical simulation techniques to the complex flow that develops near the base of a jet-propelled tactical missile or a rocket-assisted artillery projectile. This complex flow has been analyzed in the past with the help of ad-hoc "component" models, which provide relatively low-cost, approximate solutions for engineering purposes [Anon. (1969)]. The rapid gains being made in numerical modeling based on the Navier-Stokes equations, together with dropping costs of computer utilization, lead naturally to attempting the application of these techniques to the base flow problem. Specifically, successful computations of base flow with simulated jet (modeled by a solid body of appropriate shape) made at the NASA Ames Research Center [Deiwert (1981), (1982)] represent a leading step in this direction, and open the way to numerical simulation of the fully coupled near wake with gas jet.

The technical challenge is posed by the complexity of the base flow, which involves the interaction between an underexpanded propulsive jet and the recirculating flow in the near wake. In turn, the wake flow may affect the afterbody flow, causing separation of the boundary layer near the missile base, depending on the shape of the body and the base pressure that develops as a result of the jet-wake interaction. For almost all applications, turbulent flow develops in the shear layers that separate the jet, the recirculating base flow, and the free stream.

The approach adopted to meet this challenge consisted of restricting the first attempt to axisymmetric flow with a cold propulsive jet of the same gas as the free stream (both gases being thermally and calorically perfect), and using the Lockheed Viscous Implicit Solver (LVIS), a Navier-Stokes computer code already tested in a number of other applications [see Reklis, et. al. (1983)]. The effort concentrated on adding to LVIS the capability to treat the base region (i.e., to work with an L-shaped computational domain), and to incorporate two different turbulence models, of the so-called "two-equation" type, namely the k-epsilon and the k-W models (see, for instance, [Launder and Spalding (1972)]). Validation of numerical simulations is always an important aspect of their application to practical problems, and in this respect the approach adopted was to establish a "sealed envelope" test, according to which the code would be applied in a true predictive fashion to wind-tunnel tests performed at AEDC, the results of which would be unavailable to the contractor performing the numerical simulation. Thus, the LVIS code was modified as required, and applied to the specific AEDC test conditions, using both the k-epsilon and k-W turbulence models. Comparison of these results with the AEDC experimental data will be performed by MICOM, and the conclusions from this exercise will be forthcoming.

This final report includes the equations and boundary conditions used in the computer code (Section 2), the numerical solution technique (Section 3), and a description of the results of the numerical simulation computer runs made with the k-epsilon and k-W turbulence models (Section 4). The detailed data from the numerical simulations are available in magnetic tape. The instructions for using the computer code are given in a Users Manual that is contained in a separate volume.

2. EQUATION AND BOUNDARY CONDITIONS

2.1 Governing Equations

2.1.1 Flow Equations. The turbulent flow over the forebody and in the base region is assumed to be governed by the classical Navier-Stokes equations with effective values of viscosity and thermal conductivity that are the sum of laminar and turbulent contributions

$$\mu = \mu_l + \mu_t \tag{2.1a}$$

$$\frac{K}{C_p} = \frac{\mu_l}{Pr_l} + \frac{\mu_t}{Pr_t} \tag{2.1b}$$

where μ denotes the viscosity, K the thermal conductivity, C_p the heat capacity, Pr the Prandtl number, and the subscripts 1 and t refer to molecular (laminar) and turbulent quantities, respectively. In the present work, the eddy viscosity μ_t is obtained from either one of two multi-equation turbulence models, and the turbulent Prandtl number is assumed to be a constant.

The numerical solution to the described Navier-Stokes equations is carried out in a general curvilinear coordinate system. The curvilinear coordinate transformations and equations can be found in [Pulliam and Steger (1980) or in Thomas and Lombard (1970)]. The simplification of the equations for axisymmetric flow is described by [Nietubicz, et al., 1979]. In the present work, the full set of viscous terms are retained (see, for example, [Thomas (July, 1979)], including the cross-derivative terms; whereas, these terms were omitted in [Pulliam and Steger (1980)] and in [Nietubicz, et al. (1979)].

2.1.2 Turbulence Model Equations. In high Reynolds number flow regions away from walls, we employ a generalized two-equation turbulence model that embodies both the uncorrected k-epsilon model [Jones and Launder (1972), Launder and Spalding (1972), and Mace, et al., 1981] and the k-W model [Launder and Spalding (1972) and Spalding (1972)].

The generalized model equations in dimensionless form are

$$(\rho k)_t + \nabla\cdot\rho\vec{V}k - Re^{-1}\,\nabla\cdot(D_k\nabla k) = S_k$$

$$S_k = \rho\left[\nu_t\Phi - C_{Dk}\,k^{\alpha Dk}\,\Gamma^{\beta Dk}\right] \tag{2.2a}$$

$$(\rho\Gamma)_t + \nabla\cdot\rho\vec{V}\Gamma - Re^{-1}\,\nabla\cdot(D_\Gamma\nabla\Gamma) = S_\Gamma \tag{2.2b}$$

$$S_\Gamma = \rho\left[C_{P\Gamma}k^{\alpha_{\rho\Gamma}}\,\Gamma^{\beta_{\rho\Gamma}}\,\Phi + C'_{\rho\Gamma}k^{\alpha'_{\rho\Gamma}}\,\Gamma^{\beta'_{\rho\Gamma}}(\nabla\omega)^2 - C_{\rho\Gamma}k^{\alpha_{\rho\Gamma}}\,\Gamma^{\beta_{\rho\Gamma}}\right]$$

where k denotes the turbulent kinetic energy (T.K.E.), Γ represents the second turbulence model parameter (epsilon or W), D_k and D_Γ are diffusion coefficients defined in terms of the molecular and eddy viscosities and "exchange coefficients" σ that are empirical constants

$$D_k = \mu_l + \frac{\mu_t}{\sigma_k} \tag{2.3a}$$

$$D_\Gamma = \mu_l + \frac{\mu_t}{\sigma_\Gamma} \tag{2.3b}$$

and where ρ is the density, $\vec{V}$ is the flow velocity, Φ is the classical dissipation function, which can be represented in Cartesian tensor notation as

$$\Phi = \left(\frac{\partial u_i}{\partial x_j} + \frac{\partial u_j}{\partial x_i}\right) \frac{\partial u_i}{\partial x_j}$$

$\omega = \left| \nabla \times \vec{V} \right|$ is the magnitude of the vorticity vector, ν_t is a Reynolds number-scaled turbulent kinematic viscosity

$$\nu_t = C_\nu k^{\alpha_\nu} \Gamma^{\beta_\nu} \tag{2.4}$$

and the eddy viscosity is given by

$$\mu_t = Re\ \rho\ \nu_t \tag{2.5}$$

All quantities in the above equations are dimensionless, with velocity, distance, density, and viscosity normalized by some reference value for each, time non-dimensionalized by the ratio of reference length to reference velocity, turbulent kinetic energy normalized by the square of the reference velocity, Γ non-dimensionalized by the appropriate combination of reference length and velocity, and the Reynolds number Re is formed from the reference values of density, velocity, length, and viscosity. The reference conditions used in the present baseflow analysis are the freestream speed of sound, density, viscosity, temperature, and pressure; and the exit radius of the nozzle (see also Section 4).

The remaining coefficients and exponents in the foregoing turbulence model equations are constants. Dimensional analysis determines uniquely the values of the exponents in terms of the dimensions of the second turbulence parameter, Γ. If we represent the latter's dimensions in units of length L and the time T follows

$$[\Gamma] \sim L^n \, T^m$$

then the appropriate values for the two turbulence models are

k-epsilon Model: $n = 2, \; m = -3$ (2.6)

k-W Model: $n = 0, \; m = -2$

and the various exponents α, β in Eq's (2.2)-(2.5) are given by

$$\alpha_\nu = \frac{n+2m}{2(n+m)} \qquad \beta_\nu = \frac{1}{n+m} \tag{2.7a}$$

$$\alpha_{Dk} = \frac{3n+2m}{2(n+m)} \qquad \beta_{Dk} = -\frac{1}{n+m} \tag{2.7b}$$

$$\alpha_{\rho\Gamma} = -\frac{n}{2(n+m)} \qquad \beta_{\rho\Gamma} = 1 + \frac{1}{n+m} \tag{2.7c}$$

$$\alpha'_{\rho\Gamma} = \frac{n+2m}{2(n+m)} \qquad \beta'_{\rho\Gamma} = \frac{1}{n+m} \tag{2.7d}$$

$$\alpha_{D\Gamma} = \frac{n}{2(n+m)} \qquad \beta_{D\Gamma} = 1 - \frac{1}{n+m} \tag{2.7e}$$

Table 2.1 gives the values of the remaining constants in Eq's (2.2)-(2.5) for which those equations reproduce either the k-epsilon or the k-W turbulence model equations. For reference, the table also indicates the equivalent notation that normally has been used for the coefficients in previous work dealing with either turbulence model. For example, the symbol C_1 previously has been used in the k-W model literature to denote $C'_{p\Gamma}$, the empirical coefficient of $(\nabla\omega)^2$ in the second production term on the R.H.S. of Eq. (2.2b).

The turbulence model equations (2.2)-(2.5) apply only in high Reynolds number flow regions far from walls. In low-speed flow regions, such as within the boundary layers on the missile side wall and on the solid part of the base, one either must add further "wall correction" terms to the model equations, or must employ some other near-wall turbulence model. Several investigators have introduced "wall correction" terms into the k-epsilon model equations and applied the expanded models successfully to simple boundary layer flows [Jones and Launder (1972), Chien (1982)]. However, the behavior of such correction terms has yet to be investigated for complex flows with vortices, embedded shock waves, etc. Therefore, we have elected to follow the approach of [Arora, et al., (1982)], who used an algebraic mixing length model for the eddy viscosity in the near-wall region of the boundary layers, and who applied the turbulence model equations (2.2)-(2.5) only outside this region.

Table 2.1

Constants in Generalized Turbulence Model Equations (2.1) - (2.5)

	k-epsilon Model [Mace, et al (1981)]		k-W Model [Spalding (1972)]	
Constant	Value of Constant	Corresponding Symbol	Value of Constant	Corresponding Symbol
C_{ν}	0.09	C_D	1.0	---
C_{Pk}	0.09	C_D	1.0	---
C_{Dk}	1.0	---	0.09	C_D
$C_{P\Gamma}$	0.1296	$C_D C_1$	1.48	C_3
$C'_{P\Gamma}$	0.0	---	3.5	C_1
$C_{D\Gamma}$	1.92	C_2	0.17	C_2
σ_k	1.0	σ_k	0.9	σ_k
σ_Γ	1.3	σ_ε	0.9	σ_w
α_{ν}	2	---	1	---
β_{ν}	-1	---	-1/2	---
Pr_t	0.9	---	0.86	---

For smooth walls [Arora, et al. (1982)] use the van Driest eddy viscosity formulation

$$\nu_t = (0.4\ Dy)^2\ \Phi^{1/2} \tag{2.8}$$

$$D = 1 - \exp(-E)$$

where y is the distance normal to the wall. For generality, we have employed the square root of the dissipation function $\Phi^{1/2}$ instead of the wall-normal gradient of tangential velocity as used in [Arora, et al. (1982)]; the two become equal in the neighborhood of a wall.

In [Arora, et al. (1982)], the exponent E of the damping factor D is given by

$$E = \frac{y^+}{A^+}\ \frac{\tau/\nu}{\tau_w/\nu_w} = y\ \frac{Re^{1/2}}{A^+}\ \frac{\rho\Phi^{1/2}}{\left(\rho_w \mu_w \Phi_w^{1/2}\right)^{1/2}} \tag{2.9}$$

where y^+ is the distance from the wall, normalized by the viscous length scale, which is defined as the ratio of the kinematic viscosity at the wall to the friction velocity; τ is the local shear stress, and A^+ is the damping constant.

An alternative expression is the formula used for the inner near-wall region in the Baldwin-Lomax algebraic turbulence model [Baldwin and Lomax (1978)]

$$E = \frac{y+}{A+} = y\ \frac{Re^{1/2}}{A+}\ \left[\frac{\rho_w \Phi_w^{1/2}}{\mu_w}\right]^{1/2} \tag{2.10}$$

In the present work, as in [Arora, et al.,(1982)], the edge of the inner region is to be positioned just outside the laminar sublayer, y^+ 15. Boundary conditions for the two turbulence model parameters at this edge are obtained from the dual condition that the eddy viscosity must be continuous across the edge, and that the turbulent kinetic energy k is assumed to be in local equilibrium. The continuity condition gives one equation between k and Γ at the inner region edge by equating the two expressions (2.4) and (2.8) for ν_τ and the local equilibrium condition yields a second equation by setting equal to zero the source term S_k on the R.H.S. of the T.K.E. Equation (2.2a).

A general three-dimensional coordinate transformation is applied to the unsteady Navier-Stokes equations [Thomas and Lombard (1979)] and the transformed equations are simplified for axisysmmetric flow [Nietubicz, et al., (1979)]. The same transformations and simplifications are applied to the turbulence model Equations (2.2) - (2.10). If we represent the transformation in the form

$x, y, z, t \longrightarrow \xi, \eta, \zeta, \tau$

with $\tau = t$, and take η as the meridional angle in axisymmetric geometry, then the transformed turbulence model equations can be written in vector form as

$$\left(J\rho\vec{Q}\right)_\tau + \left[\left(J\rho\vec{V}\cdot\nabla\xi\right)\vec{Q}\right]_\xi + \left[\left(J\rho\vec{V}\cdot\nabla\zeta\right)\vec{Q}\right]_\zeta - Re^{-1}\left[D_1\vec{Q}_\xi + D_3\vec{Q}_\zeta\right]_\xi \tag{2.11a}$$

$$-Re^{-1}\left[D_2\vec{Q}_\zeta + D_3\vec{Q}_\xi\right]_\zeta = \vec{S}$$

$$\vec{Q} = \begin{pmatrix} k \\ \Gamma \end{pmatrix} \quad \vec{S} = J\begin{pmatrix} S_k \\ S_\Gamma \end{pmatrix} \tag{2.11b}$$

$$D_1 = \left(\nabla\xi\right)^2 D \qquad D_2 = \left(\nabla\zeta\right)^2 D \qquad D_3 = \left(\nabla\xi\cdot\nabla\eta\right) D \tag{2.11c}$$

and where $J = \partial(x,y,z)/\partial(\xi,\eta,\zeta)$ is the Jacobian of the inverse transformation, and D is a diagonal diffusion coefficient matrix

$$D = \begin{pmatrix} D_k & 0 \\ 0 & D_\Gamma \end{pmatrix} \tag{2.11d}$$

3. NUMERICAL SOLUTION TECHNIQUE

The numerical solution to the described equations is carried out using the Beam-Warming time-linearized implicit approximate-factorization (ADI) scheme [Beam and Warming, (1978)]. When this scheme is used with algebraic turbulence models, the usual practice is to treat both laminar and turbulent transport properties as locally constant over a time step $\Delta\tau$, and then to update these quantities at the end of the step. Details of the implicit scheme applied in this fashion in curvilinear coordinates are given in [Pulliam and Steger, (1980)]. For multi-equation turbulence models such as employed here, one could solve the entire system of flow and turbulence model equations directly by the implicit numerical scheme, but this would be both cumbersome and computationally inefficient. Instead, we invoke a few simple approximations that do not affect the accuracy of the steady state solutions of interest here, and that both simplify the scheme and improve the computational efficiency. These approximations and the resulting computational procedure are described below.

3.1 Flowfield Difference Equations. The flowfield equations depend on the turbulence model parameters k, Γ only through the eddy viscosity μ_t. As with algebraic turbulence models, we neglect this dependence to first order by treating μ_t as locally constant over a step $\Delta\tau$. This allows the flowfield and turbulence model equations to be solved in tandem, rather than simultaneously. The flow equations are solved first in the usual way [Thomas and Lombard (1979), Pulliam and Steger (1980)] to obtain the time differences ΔP, $\Delta\vec{V}$ and the updated flow variables p^{n+1}, $\vec{V}^{n+1}$, etc. These values then are used in the subsequent solution of the turbulence model equations by essentially the same implicit scheme.

3.2 Turbulence Model Difference Equations. We employ the first-order Euler-implicit time differencing scheme. The time-linearized difference equations for Eq. (2.11) then can be written in the form

$$\left\{ aI + \Delta\tau \left[\mu_1 \delta_1 bI + \mu_j \delta_j eI - Re^{-1}\left(\delta_1 \frac{\partial \vec{T}_1}{\partial \vec{Q}} + \delta_j \frac{\partial \vec{T}_2}{\partial \vec{Q}} \right) - \frac{\partial \vec{S}}{\partial \vec{Q}} \right] \right\} \Delta\vec{Q} \qquad (3.1a)$$

$$= -\vec{Q}^n \Delta a - \vec{R}\Delta\tau$$

$$a = (j\rho)^{n+1},\ b = a(\vec{V}\cdot\nabla\xi)^{n+1},\ c = a(\vec{V}\cdot\nabla\xi)^{n+1} \qquad (3.1b)$$

$$\vec{R} = \mu_1 \delta_1 b\vec{Q}^n + \mu_j \delta_j c\vec{Q}^n - Re^{-1}\left[\delta_1 \vec{T}_1^n + \delta_j \vec{T}_2^n + \mu_1 \delta_1 \vec{T}_3^n + \mu_j \delta_j \vec{T}_4^n \right] \qquad (3.1c)$$

$$\vec{T}_1 = D_1 \delta_1 \vec{Q},\ \vec{T}_2 = D_2 \delta_j \vec{Q},\ \vec{T}_3 = D_3 \mu_j \delta_j \vec{Q},\ \vec{T}_4 = D_3 \mu_1 \delta_1 \vec{Q} \qquad (3.1d)$$

$$\xi_i = (i-1)\Delta_1\xi,\ \zeta_j = (j-1)\Delta_j\zeta,\ \Delta_1\xi = \Delta_j\zeta = 1 \qquad (3.1e)$$

in which I is the identity operator (matrix) and $\Delta\vec{Q}$ is the only unknown. Here, we have employed classical difference operator notation Δ, δ, $\mu\delta$ with a subscript on each spatial operator to distinguish the direction in which that operator acts. For example, for a mesh function f^n_{ij}, the spatial operators are defined as follows

$$\Delta_1 f = f^n_{i+1,j} - f^n_{i,j}$$

$$\mu_1 \delta_1 f = \left(f^n_{i+1,j} - f^n_{i-1,j}\right)\Big/2 \tag{3.2}$$

$$\delta_1 f = f^n_{i+1/2} - f^n_{i-1/2}$$

and Δ without a subscript represents the forward time difference operator

$$\Delta f = f^{n+1}_{ij} - f^n_{ij} \tag{3.3}$$

Following [Beam and Warming (1978)], the diffusive cross-derivative terms have been treated in explicit fashion in Equation (3.1). For later reference, we note that difference equation (3.1a) does not contain artificial smoothing terms.

To simplify the solution of the difference equations (3.1), we perform an approximate factorization of the implicit L.H.S. operator into three parts. Two of these are the usual one-dimensional factors for each coordinate direction, and the third involves only the source-term Jacobian matrix $d\vec{S}/d\vec{Q}$. The factored-operator form of Equation (3.1) is

$$\left[aI + \Delta\tau\left(\mu_1 \delta_1 bI - Re^{-1}\delta_1 \frac{\partial\vec{T}_1}{\partial\vec{Q}}\right)\right]\Delta\vec{Q}^{**} = -\vec{Q}^n\Delta a - \vec{R}\Delta\tau$$

$$\left[aI + \Delta\tau\left(\mu_j \delta_j cI - Re^{-1}\ \delta_j \frac{\partial\vec{T}_2}{\partial\vec{Q}}\right)\right]\Delta\vec{Q}^{*} = a\Delta\vec{Q}^{**} \tag{3.4}$$

$$\left[aI + \Delta\tau\frac{\partial\vec{S}}{\partial\vec{Q}}\right]\Delta\vec{Q} = a\Delta\vec{Q}^{*}$$

The implicit operator inversion sequence thus involves two successive block-tridiagonal matrix inversions, one for each spatial direction, followed by a block-explicit matrix inversion locally at each grid point, where each block has only a dimension of 2. In each of the spatial block-tridiagonals, the two equations (for the two components of $\vec{Q}$) are coupled only through the turbulent viscosity μ_t. The block-tridiagonal then is reduced to a set of two easily-inverted scaler tridiagonal equations upon approximating μ_t as locally constant over a time step, which is the same approximation employed in treating the flow equations themselves. Note that this approximation also renders the diffusion terms $\vec{T}_1$ and $\vec{T}_2$ linear in $\vec{Q}$, and their Jacobian matrices take the simple form

$$\frac{\partial \vec{T}_1}{\partial \vec{Q}} = D_1^n \qquad \frac{\partial \vec{T}_2}{\partial \vec{Q}} = D_2^n \tag{3.5}$$

Numerical experiments have revealed that the described algorithm for the turbulence model equations is both stable and accurate in regions where the turbulence level is significant, such as in a boundary layer, shear layer, or jet mixing layer. However, numerical difficulties, usually in the form of slightly negative values of the turbulence energy k, often arise in low-turbulence regions where μ_t in Equation (2.1) is insignificant. An example is the approximately uniform near-freestream flow region radially far from the missile afterbody wall in Figure 3.1, where k and μ_t are very small. These difficulties have been overcome by employing upwind rather than central difference operators in the advective terms involving $\vec{V}$ on both right-hand and left-hand sides of the difference equation (3.4). The implementation for the turbulence model equations follows that described in [Reklis and Thomas (1981)] for the Euler equations.

3.3 Boundary Conditions. Boundary conditions for the flow variables and turbulence model parameters at the various boundaries depicted in Figure 3.1 were determined and applied as described below.

Implicit boundary conditions at the outflow plane and at the symmetry axis were computed as described in [Thomas and Lombard (1979)]. The remaining boundary conditions were applied in explicit fashion; that is, they were maintained as locally constant over a time step and then updated at the end of the step. No-slip adiabatic wall boundary conditions were used at the missile sidewall and along the solid part of the base. The pressure and temperature at each grid point along the wall were updated by setting them equal to the values at the adjacent interior point. Boundary conditions for the two turbulence model parameters are not applied at the wall, but at the edge of the near-wall region within which the algebraic eddy viscosity model (2.8) is used. The edge of the near-wall ($y^+ \approx 15$). Boundary values of k and Γ at the edge were obtained from the dual requirement that μ_t be continuous and that k be in local equilibrium, as explained earlier.

Boundary conditions at the inflow boundary and shock were derived from independent numerical solutions for the external flow over the missile

forebody and for the internal nozzle flow, and were held fixed during the baseflow computation. The forebody flow solution was computed with a 2-D axisymmetric flow version of the LVIS (Lockheed Viscous Implicit Solver) program described in [Reklis, Conti, and Thomas (1983)]. The shape of the outer bow shock wave and the flow conditions at the shock were obtained from the same solution for a fictitiously lengthened body extending to the outflow plane of Figure 3.1.

Inflow boundary conditions at the nozzle exit were obtained from a Navier-Stokes internal flow solution using the NOZL3D code [Thomas (Sept., 1979) and (1980) and Thomas and Neier (1980)] in a recent version that includes an axisymmetric flow option. The geometry of the nozzle is shown in Figure 3.2, along with the curvilinear grid used from the NOZL3D code solution. Plots of selected exit-plane flow profiles from the latter solution are displayed in Figures 3.3 to 3.5 to demonstrate the significant radial nonuniformity of the jet produced by this particular nozzle. For example, the exit-plane pressure is about 20 percent higher at the axis of symmetry than at the nozzle lip. In these figures, the radius z is normalized by the nozzle exit radius; pressure and temperature are normalized by the corresponding stagnation chamber conditions, and velocities by the stagnation sound speed.

The described numerical solutions for the external forebody flow and the internal nozzle flow employed the Baldwin-Lomax turbulence model [Baldwin and Lomax, (1978)]. Because this model is algebraic, it cannot directly yield inflow boundary conditions on the turbulence model parameters k and Γ. It was necessary to derive the latter boundary conditions with the same technique described earlier for determining the values of k and Γ at the edge of the near-wall region of the boundary layer. In the case of the inflow boundary, the known value of μ_t from the Baldwin-Lomax model and the assumption that k be in local equilibrium at each point allow deduction of local values for k and Γ. This procedure made it necessary to employ Equation (2.10) for the damping factor exponent, which is consistent with the Baldwin-Lomax model, in order to ensure continuity of the k and Γ distributions in the neighborhood of the inflow boundaries.

The same approach was used to derive boundary conditions for k and Γ at grid points just inside the bow shock boundary.

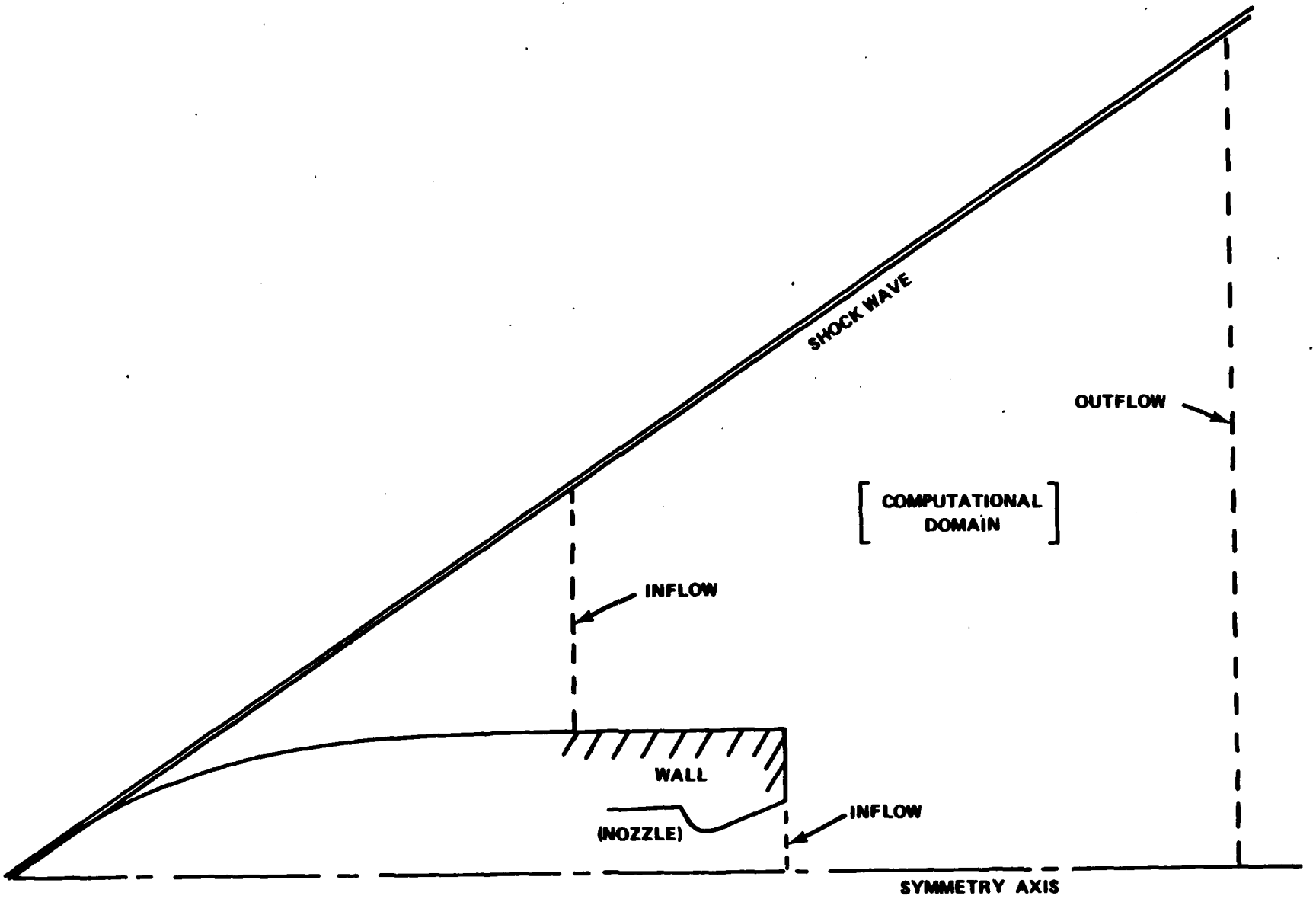

Figure 3.1. Computational domain for base flow numerical simulations.

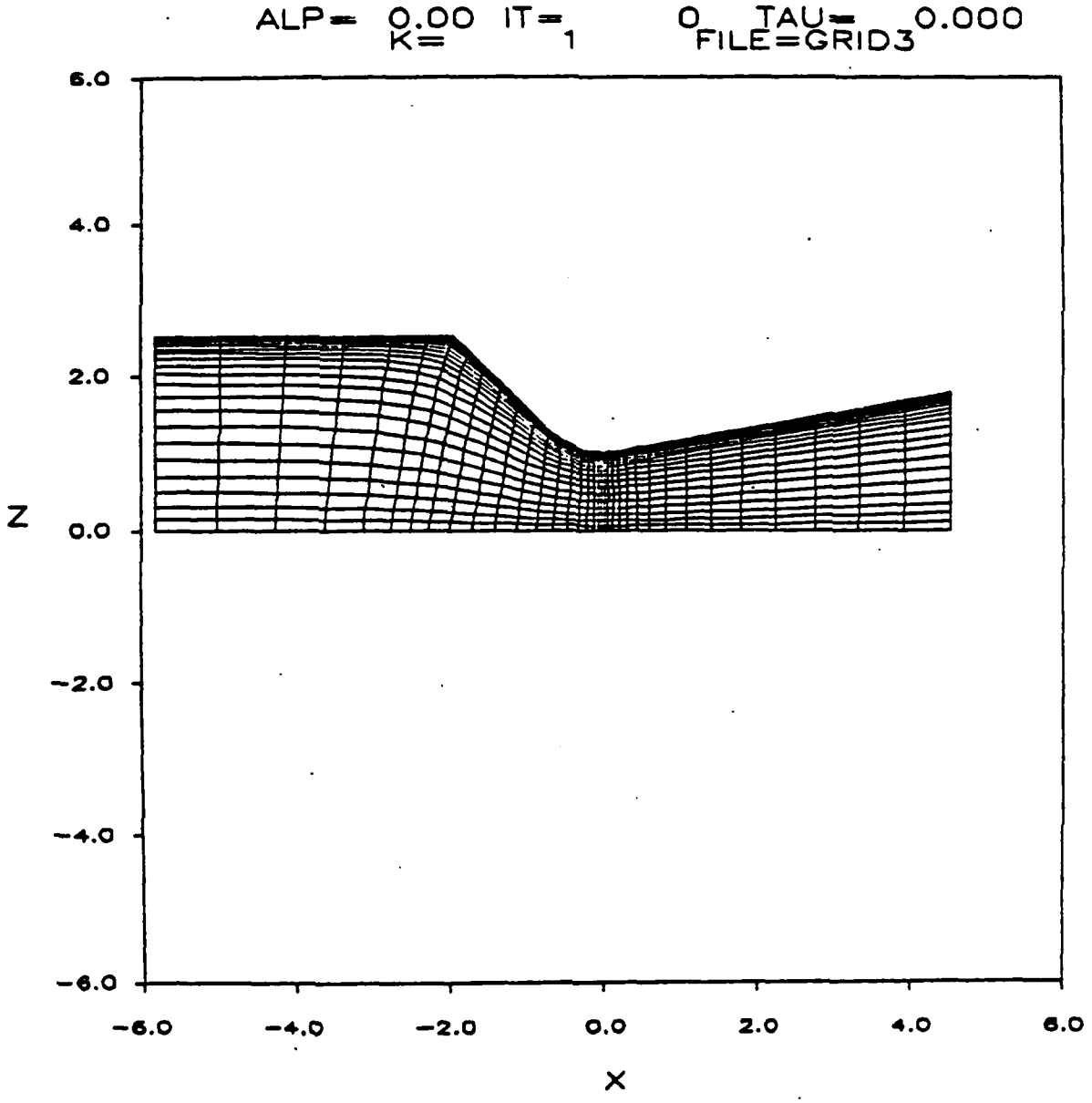

Figure 3.2. Nozzle configuration and curvilinear grid for NOZL3D code computation.

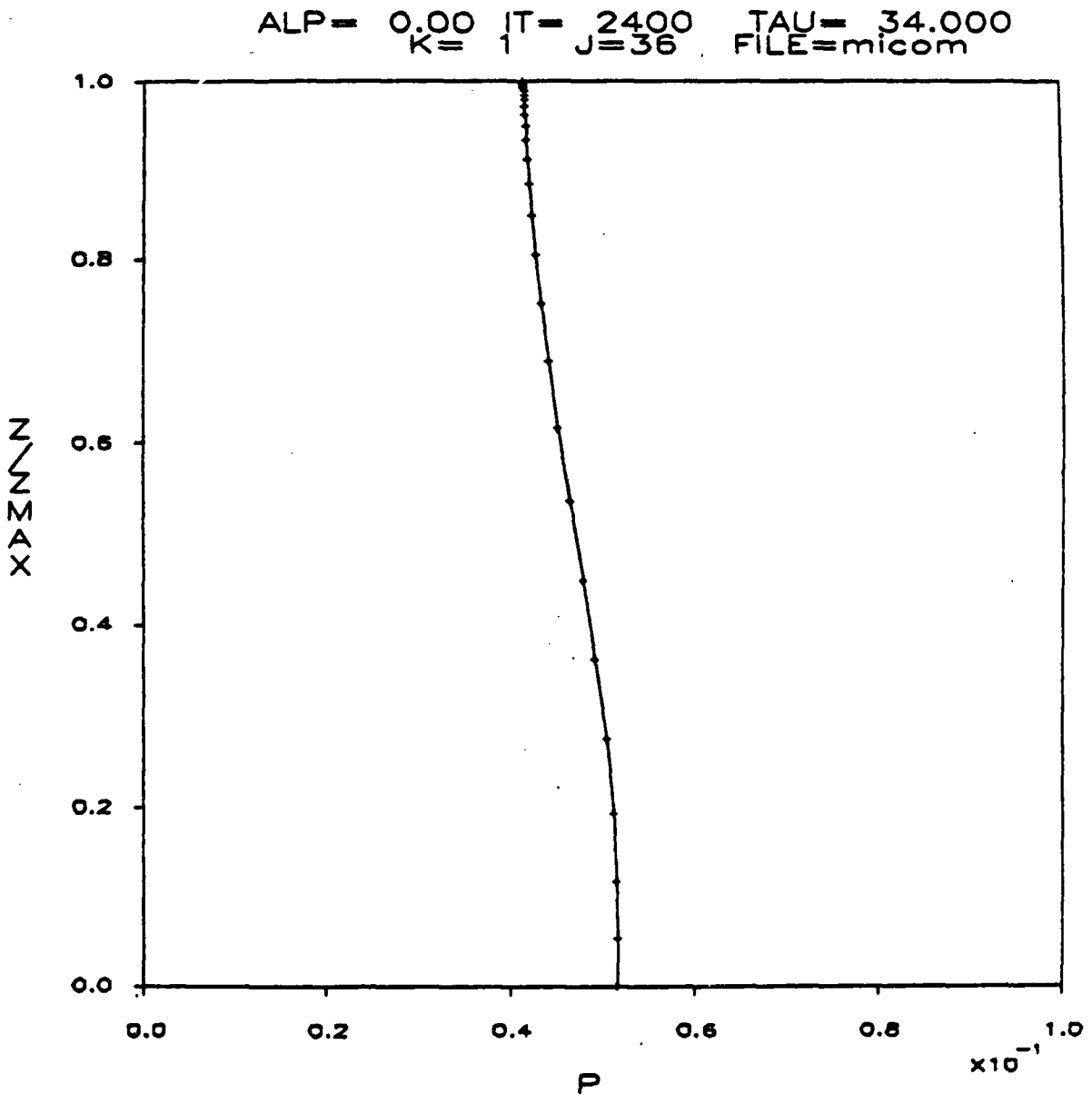

Figure 3.3. Radial profile of pressure at nozzle exit plane.

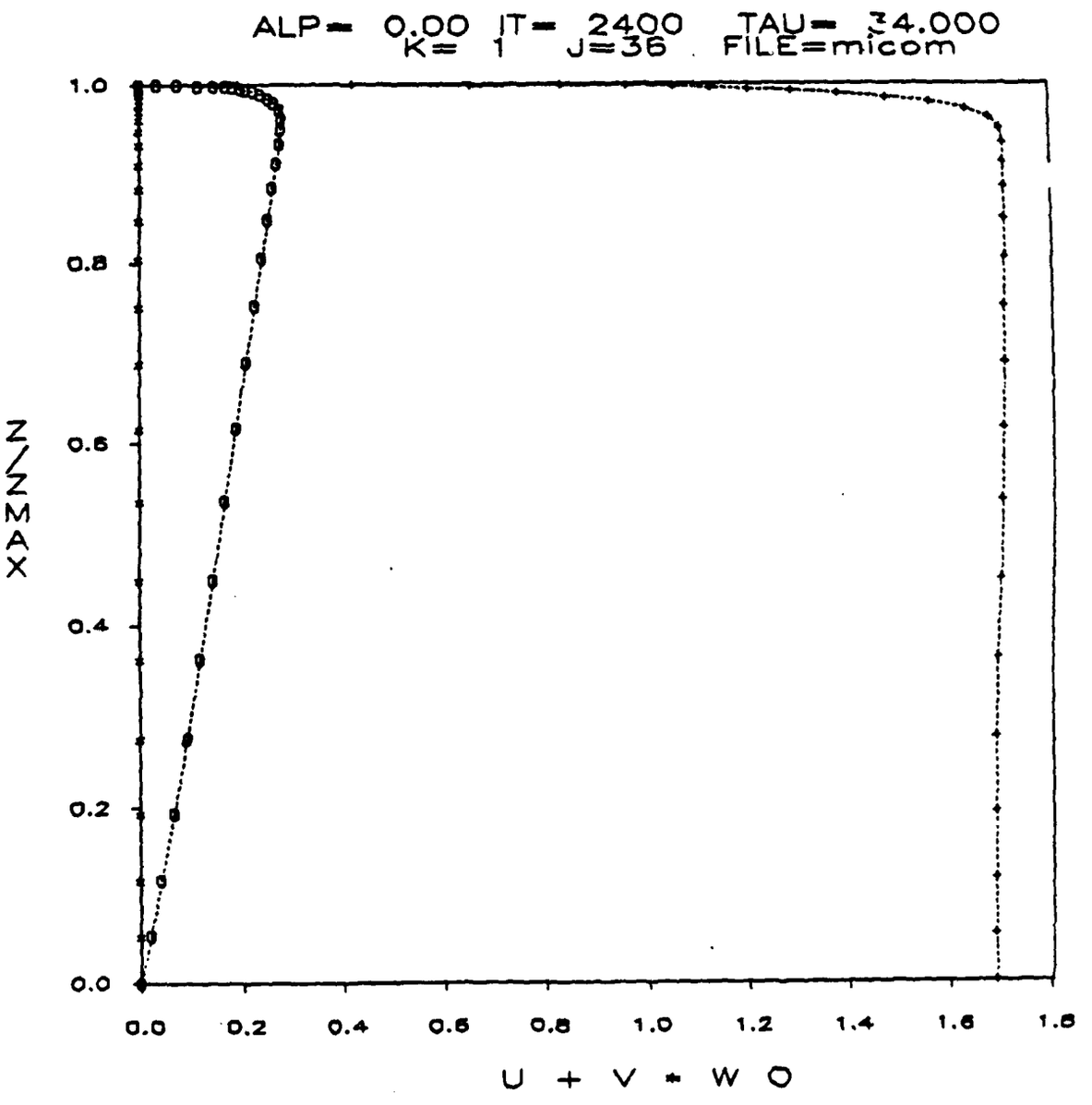

Figure 3.4. Radial profiles of velocity at nozzle exit plane: (U) axial component and (W) radial component.

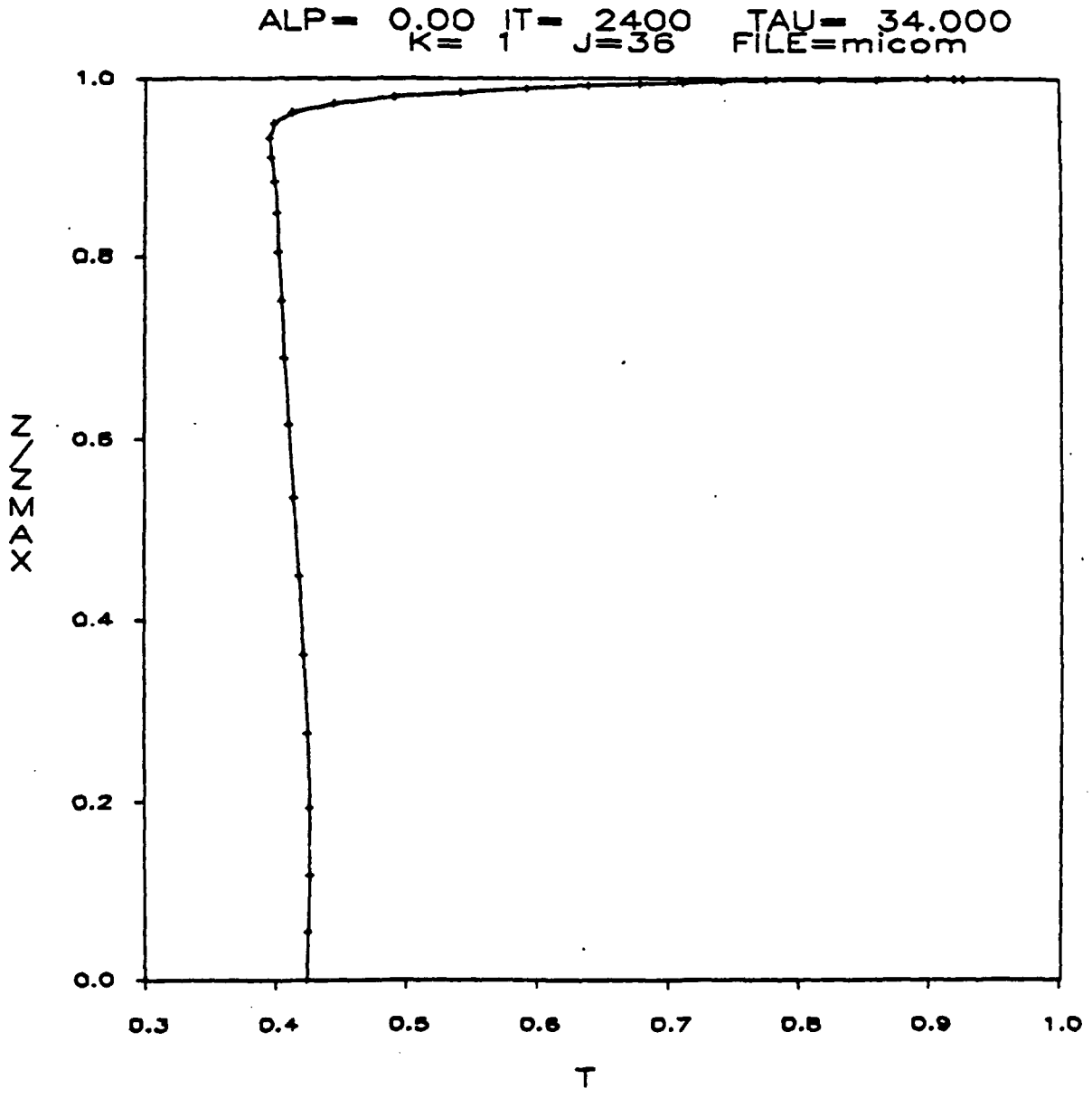

Figure 3.5. Radial profile of temperature at nozzle exit plane.

4. RESULTS OF TEST CASES

4.1 General. The test cases computed consisted of verification of the turbulence models in a boundary layer, and simulation of the flowfield corresponding to the AEDC wind-tunnel experiments. In order to make this a true prediction, the results of the AEDC measurements have not been released as of this writing; comparison of the present results with that data will be made by MICOM in the future.

Computations were made on a VAX 11/780 minicomputer and CRAY 1s mainframe. The same code (with minor modifications) was used in both computers, and on occasion the computation was moved from one computer to the other for operational convenience. Many of the runs were of experimental nature, and the cumulative running time was not computed. The running time of a "production" run can be estimated by noting that the code runs approximately 17 milliseconds per grid point per time iteration on the VAX computer.

4.2 Check of Turbulence Models. The correct operation of the turbulence models was checked by computing the flow in the boundary layer on a cylinder aligned with the free stream. This case was selected for convenience, since the base flow code is set up to compute such a flow on the aft section of a missile. Three runs were made, using the Baldwin-Lomax algebraic model, the k-epsilon model, and the k-W model, respectively. The parameters used in the two-equation models (see Table 2.1) were those corresponding to axisymmetric flow, even though a more faithful modeling of this particular flow should use the parameters recommended for two-dimensional flows with planar symmetry. The axisymmetric flow parameters were used because in the computation of base flows these were the parameters to be used thorughout the flowfield, including the boundary layer on the side walls of the missile.

All computations yielded essentially the same pressure profile. The longitudinal velocity profiles are shown on Figure 4.1. The k-W and algebraic models produced essentially the same velocity profile, but the k-epsilon model gave a fuller velocity profile in the region extending from about 2 percent to 15 percent of the boundary-layer thickness. This behavior was also observed in the density profiles, shown on Figure 4.2. The turbulent viscosity μ_t (defined in equation 2.1a) is shown on Figure 4.3. Here again the algebraic and k-W models agree well, but the k-epsilon model shows significantly larger viscosity in the region extending from about 3 percent to 42 percent of the boundary-layer thickness.

The reason for the discrepancies shown by the k-epsilon model remains obscure, but the general results of these tests indicate that the two-equation models are operational and yield reasonable solutions. Further judgment on the performance of these models is beyond the scope of this study.

4.3 AEDC Test Case

4.3.1 Discretization Grid. The grid used in the computations is shown on Figure 4.4. This grid was generated using the technique described in [Thomas (Sept. 1979)], which is based on the solution of a special set of elliptic differential equations. A computer code (RGRID) that implements this grid generation technique is provided separately [Thomas and Neier (1980)].

The grid used for the test cases has active 3216 nodes. High resolution is provided in the boundary layer on the side and base of the missile, and in the shear layers that separate the jet from the recirculating flow and the free stream. In order to economize grid points, the resolution was decreased in the upper region of the flowfield, especially above z=8, which is the upper boundary of the region surveyed in the AEDC experiments, Therefore, care must be used in interpreting the computed results in this upper region.

4.3.2 Boundary and Initial Conditions. The boundary conditions are described in detail in Paragraph 3.3. The inflow boundary conditions on the afterbody, at x=-16, were obtained from a separate forebody solution, and they match closely the boundary data from the AEDC tests. The inflow boundary condition at the nozzle exit was obtained from a nozzle computation, as discussed in Paragraph 3.3 and displayed in Figures 3.2-3.5.

The initial flowfield to start the computation was obtained from a laminar flow solution computed on a coarse, rectangular grid. The turbulence parameters were estimated roughly by interpolation of their boundary values.

The free-stream parameters used in both the k-epsilon and k-W solutions were as follows:

Mach number=1.343

Reynolds number=92320

Prandtl number=0.7

Ratio of specific heats=1.4

Static temperature=265.3 K.

The values of the constants used in the turbulence models are given in Table 2.1.

4.3.3 Time-Asymptotic Convergence. The code was run with the k-W model from the initial conditions to a dimensionless time (see definition in Paragraph 2.1.2) of approximately 28, until no appreciable changes occurred in the flow variables throughout the flowfield. Then the k-epsilon model was run, using as initial conditions the k-W solution as a dimensionless time of approximately 8. The k-epsilon solution was run to a dimensionless time of approximately 23, which is roughly equivalent to the age of the k-W solution, because of its later starting point. This solution was also converged, in the sense that no further changes were observed in the flow variables.

4.3.4 Computed Flowfield. The k-W solution will be discussed first. The flow variables are nondimensionalized as described in Paragraph 2.1.2; in particular, the coordinates are referenced to the nozzle exit radius. Figure 4.5 shows the general structure of the flowfield, as indicated by velocity vector plots. The nozzle exit extends from the centerline (z=0) to z=1; the base of the body extends to z=5. The near wake exhibits a recirculation region, which extends longitudinally to approximately x=6. Within it there is a dividing streamline that separates the upper and lower recirculating flows, with a stagnation point on the base of the missile at approximately z=2.9. The shear layers that separate the slow wake flow from the jet and the external stream are clearly visible in Figures 4.5(a), (b), and (c), which illustrate their evolution and merging along the wake.

Two minor anomalies remain unexplained: the notch in the velocity profile on the jet side of the shear layer, particularly visible in Figure 4.5(a); and the velocity defect on the axis of symmetry, which may be related to the axial-symmetry boundary condition.

Dimensionless pressure and density contours are shown in Figures 4.6 and 4.7, respectively. The density contours demarcate clearly the "edge" of the jet, as Figure 4.7 shows.

The k-epsilon solution is very similar to the k-W one. Figures 4.8(a), (b), and (c) show the velocity vector plots, and Figures 4.9 and 4.10 show the pressure and density contours, respectively. One difference with the k-W solution is that the k-epsilon recirculating region is shorter by about one nozzle exit radius. Other differences are the greater width of the k-epsilon shear layers, and the more nearly linear velocity profile of its jet, particularly downstream. These differences are consistent with the larger eddy viscosity predicted by the k-epsilon model, as illustrated by Figure 4.11, which shows profiles of the turbulent viscosity {mu sub tee} at two axial stations.

The computed results discussed in this section are available on magnetic tape, both on the original grid described in Paragraph 4.3.1 and on the grid surveyed in the AEDC wind-tunnel tests.

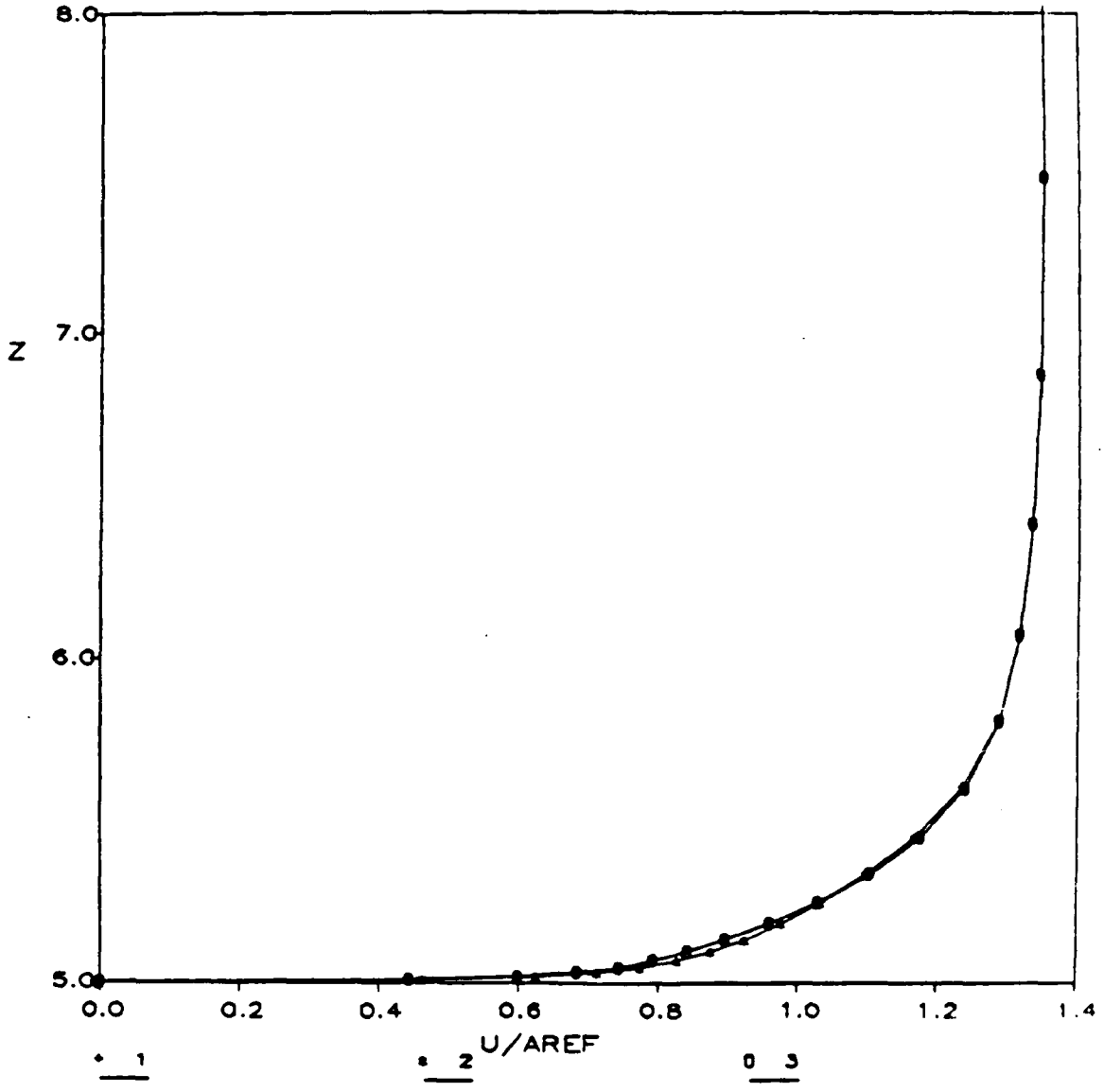

Figure 4.1. Comparison of computed boundary layer velocity profiles for three turbulence models: (1) Baldwin-Lomax algebraic model, (2) k-epsilon model, (3) k-W model.

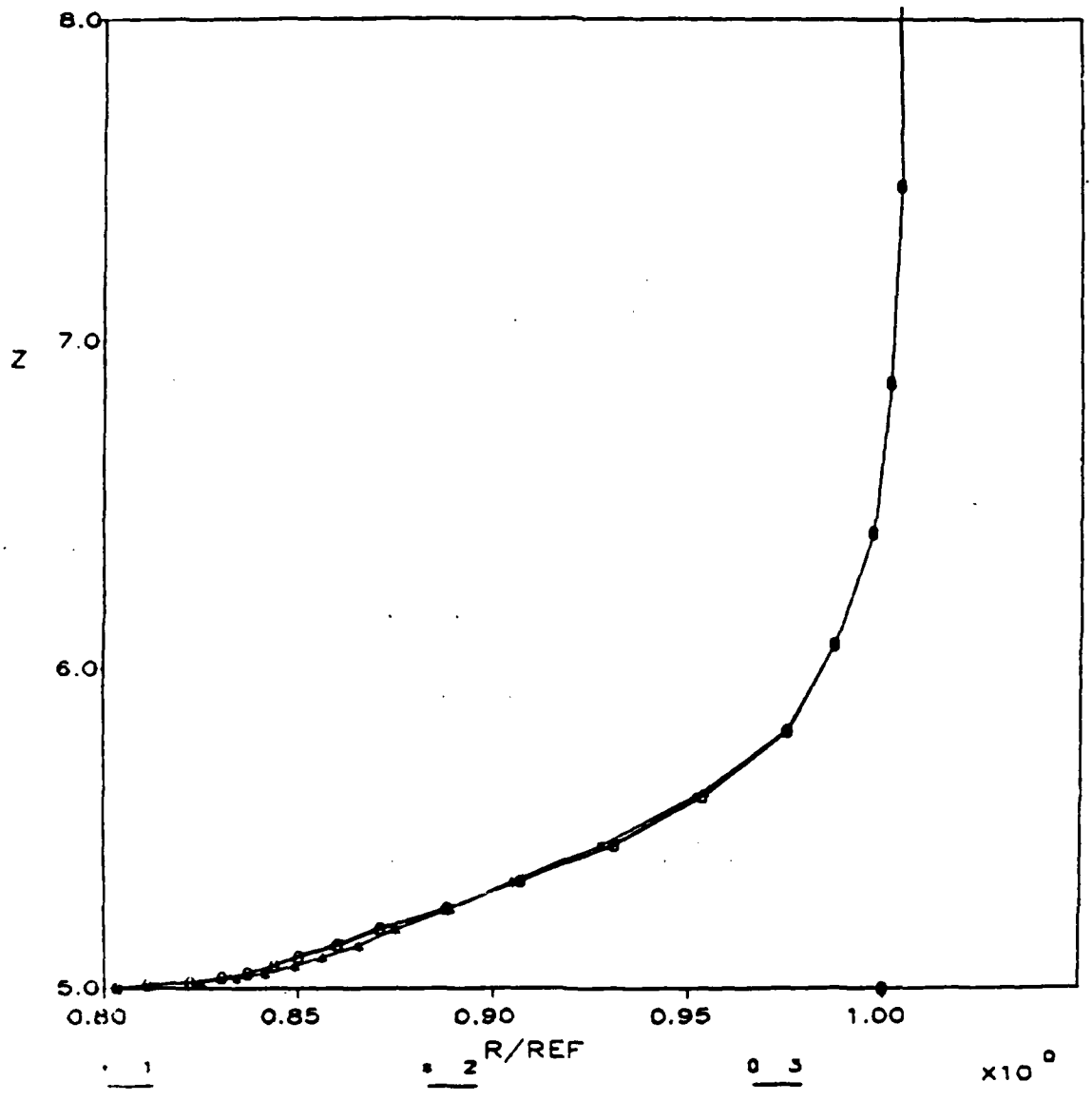

Figure 4.2. Comparison of computed boundary layer density profiles for three turbulence models: (1) Baldwin-Lomax algebraic model, (2) k-epsilon model, (3) k-W model.

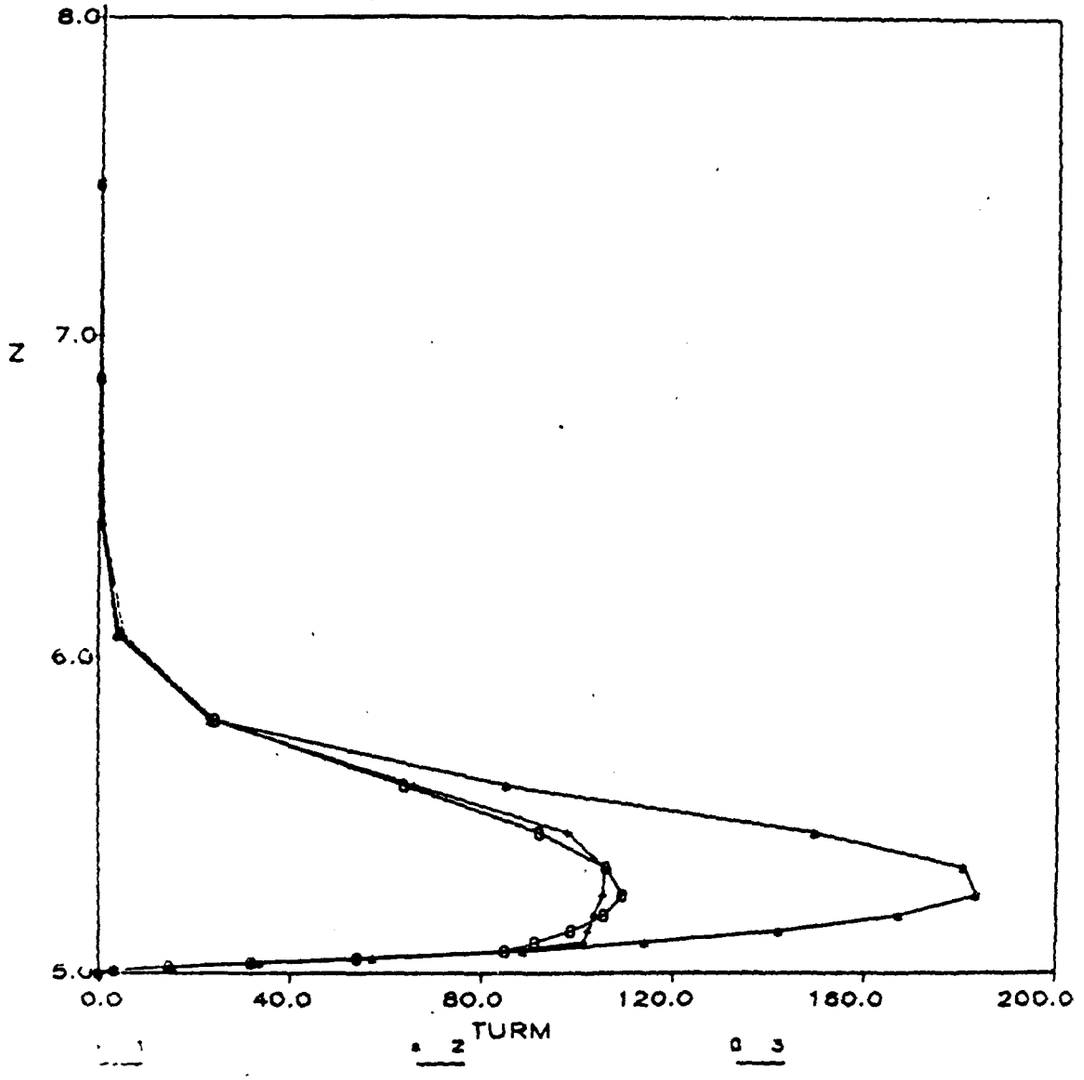

Figure 4.3. Comparison of computed boundary layer turbulent eddy viscosity profiles for three turbulence models: (1) Baldwin-Lomax algebraic model, (2) k-epsilon model, (3) k-W model.

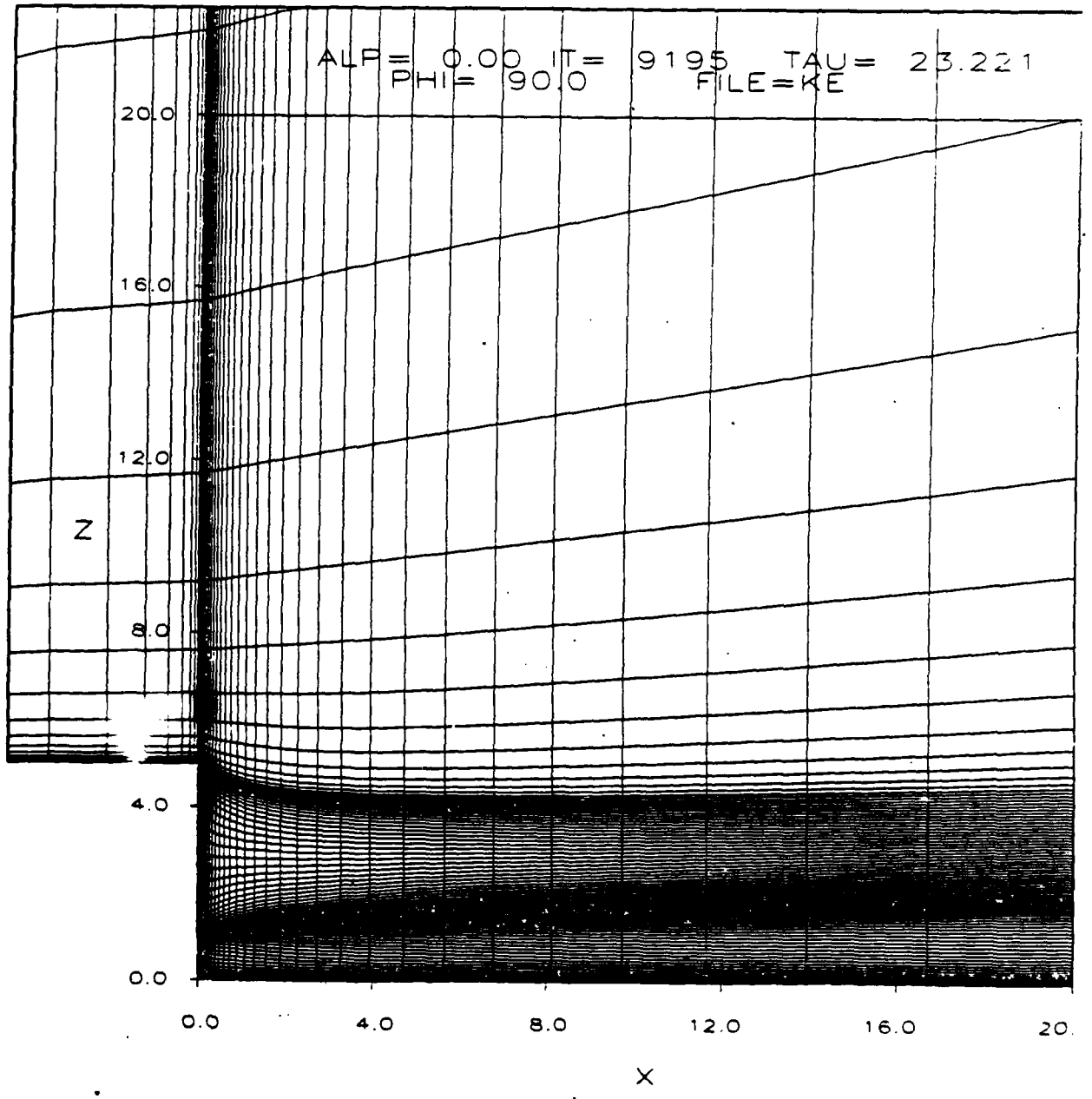

Figure 4.4. Curvilinear grid used in base flow numerical simulations.

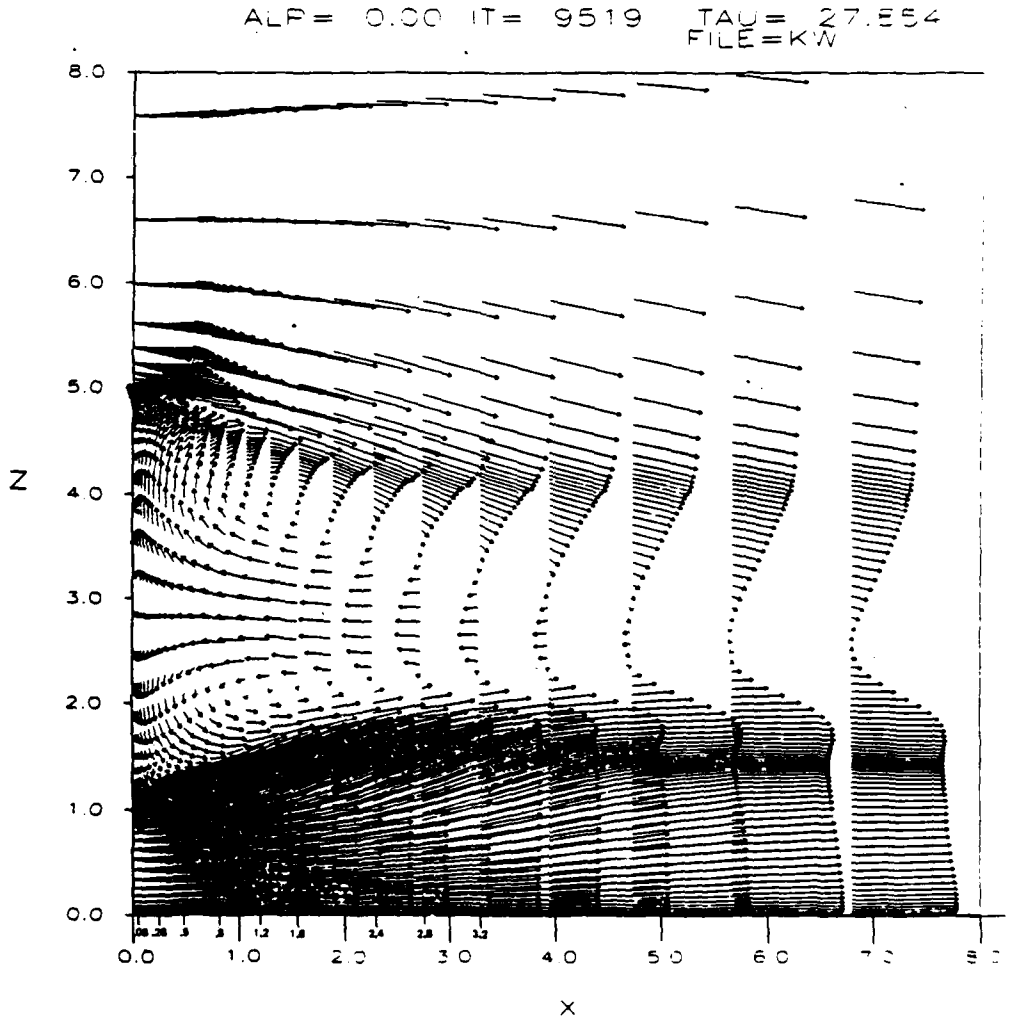

Figure 4.5(a). Velocity vectors in region downstream of base, k-W turbulence model.

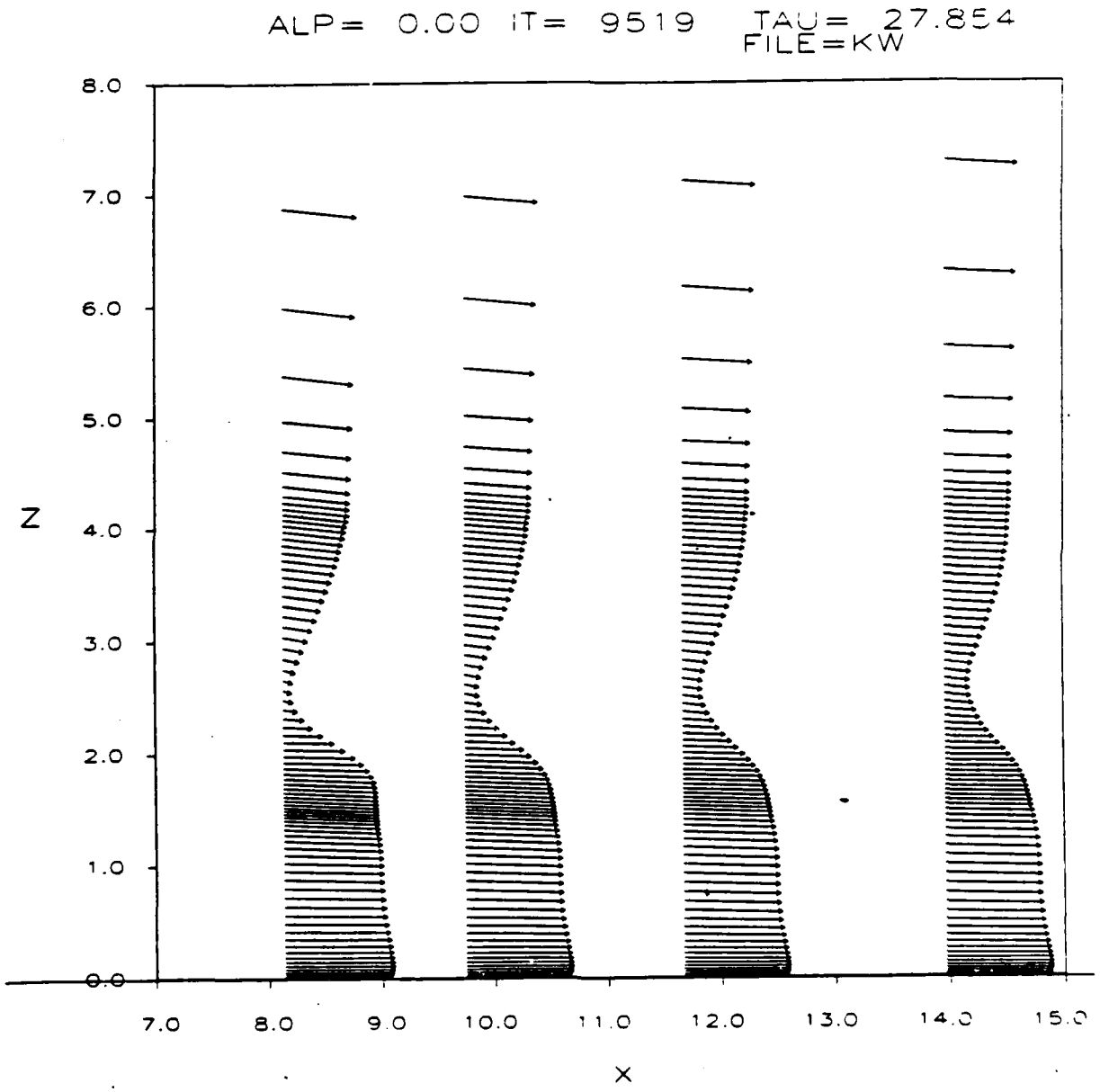

Figure 4.5(b). Velocity vectors in region downstream of base, k-W turbulence model.

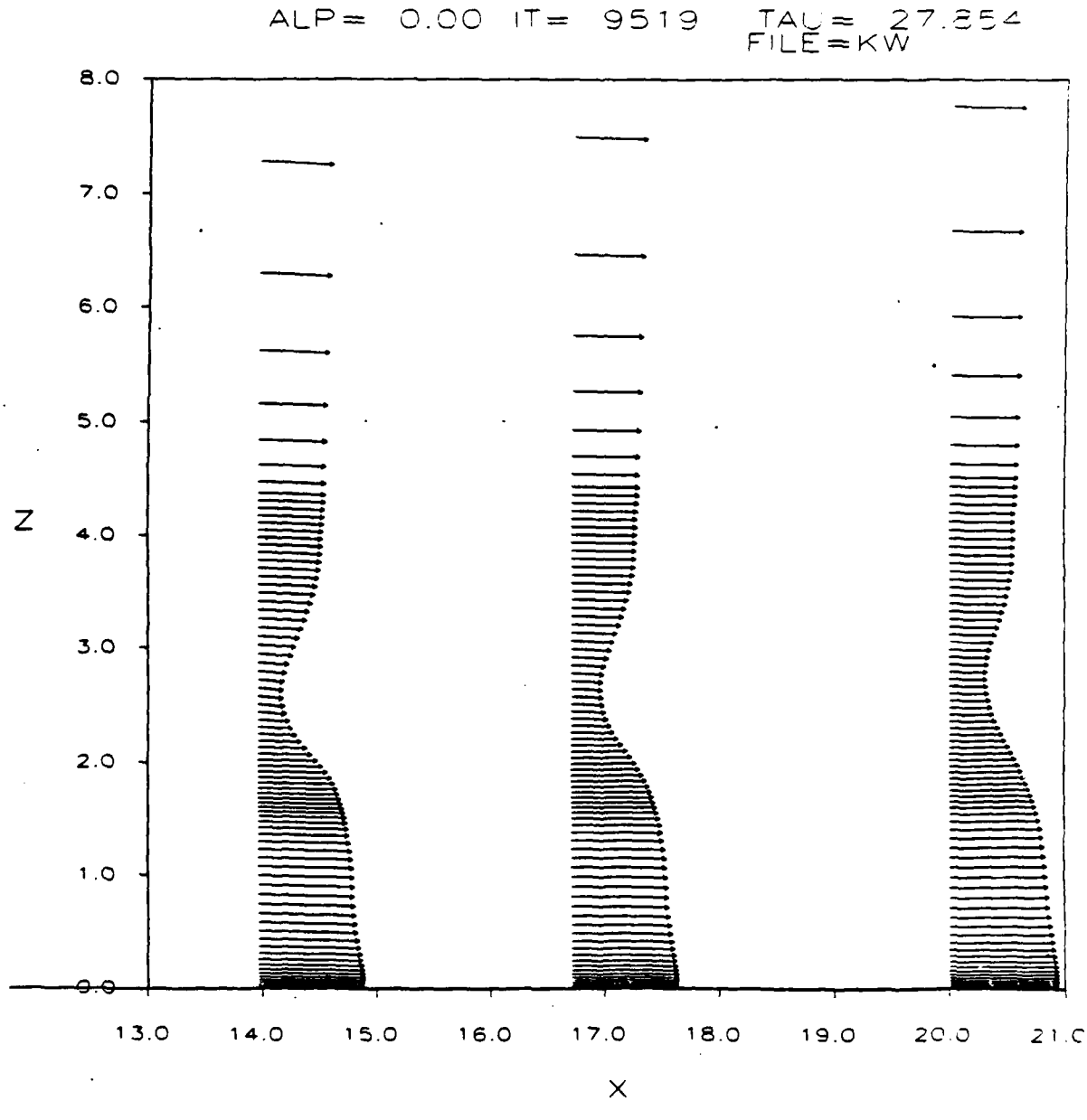

Figure 4.5(c). Velocity vectors in region downstream of base, k-W turbulence model.

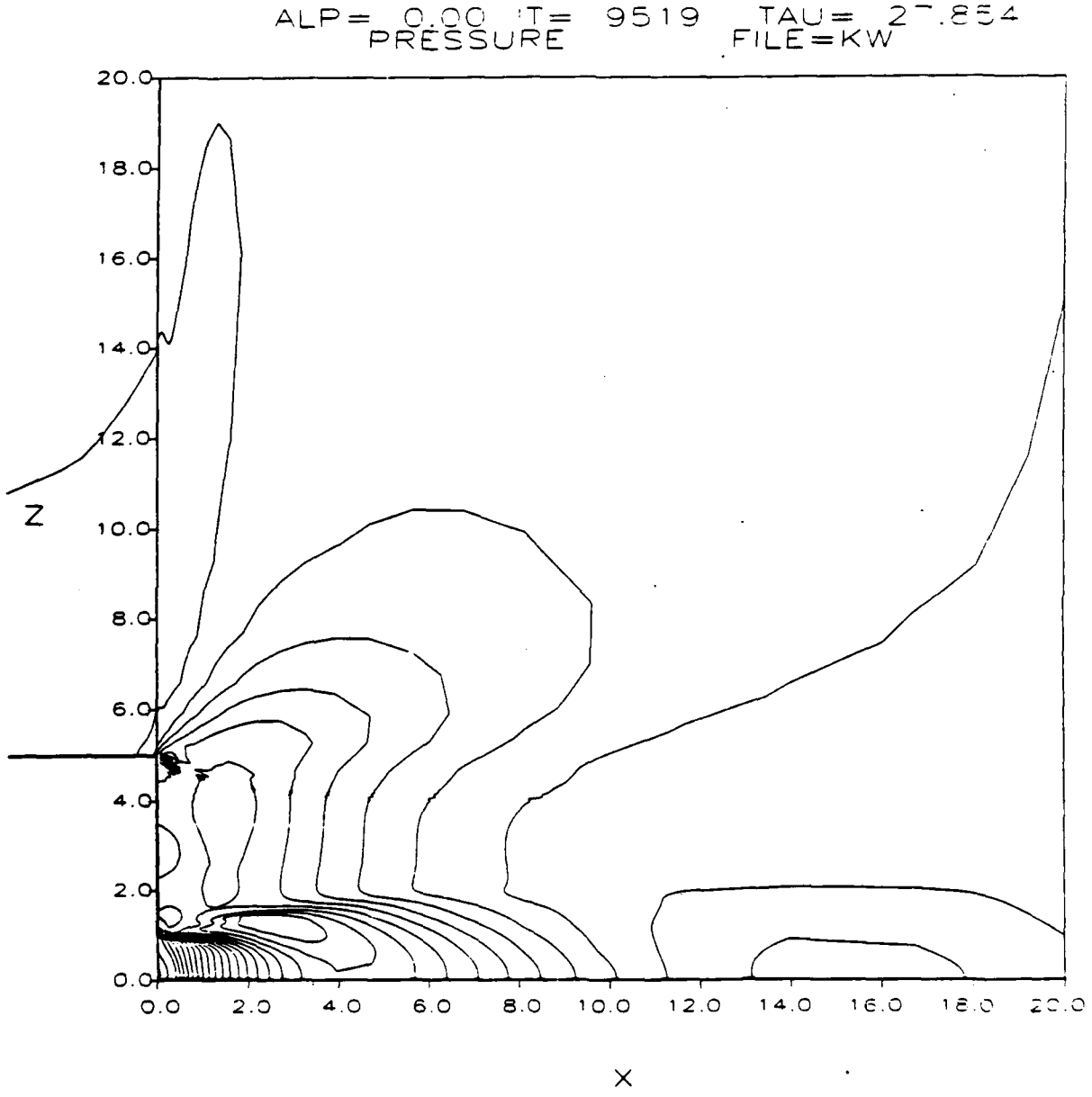

Figure 4.6. Pressure contours in base flow region, k-W turbulence model.

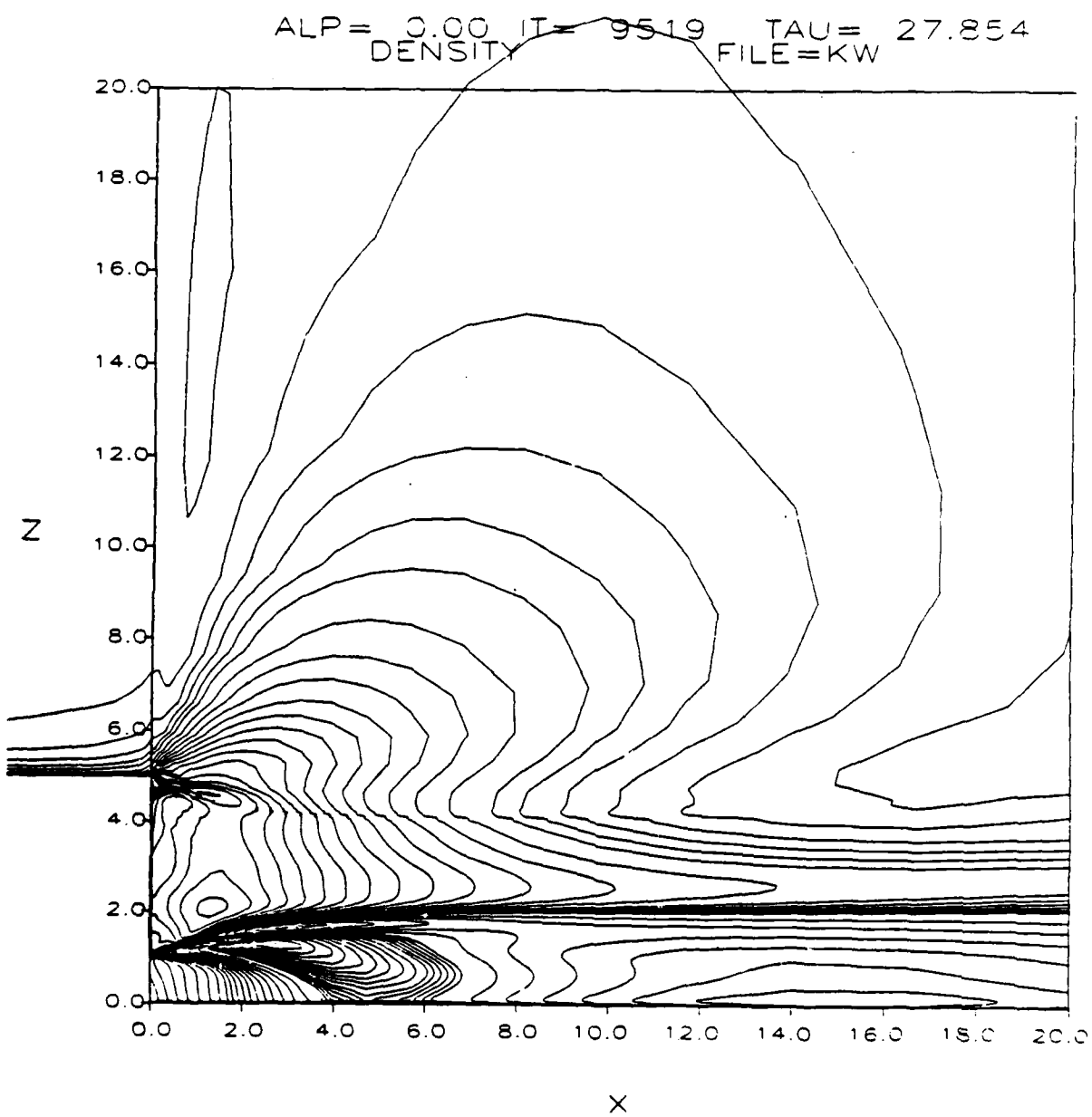

Figure 4.7. Density contours in base flow region, k-W turbulence model.

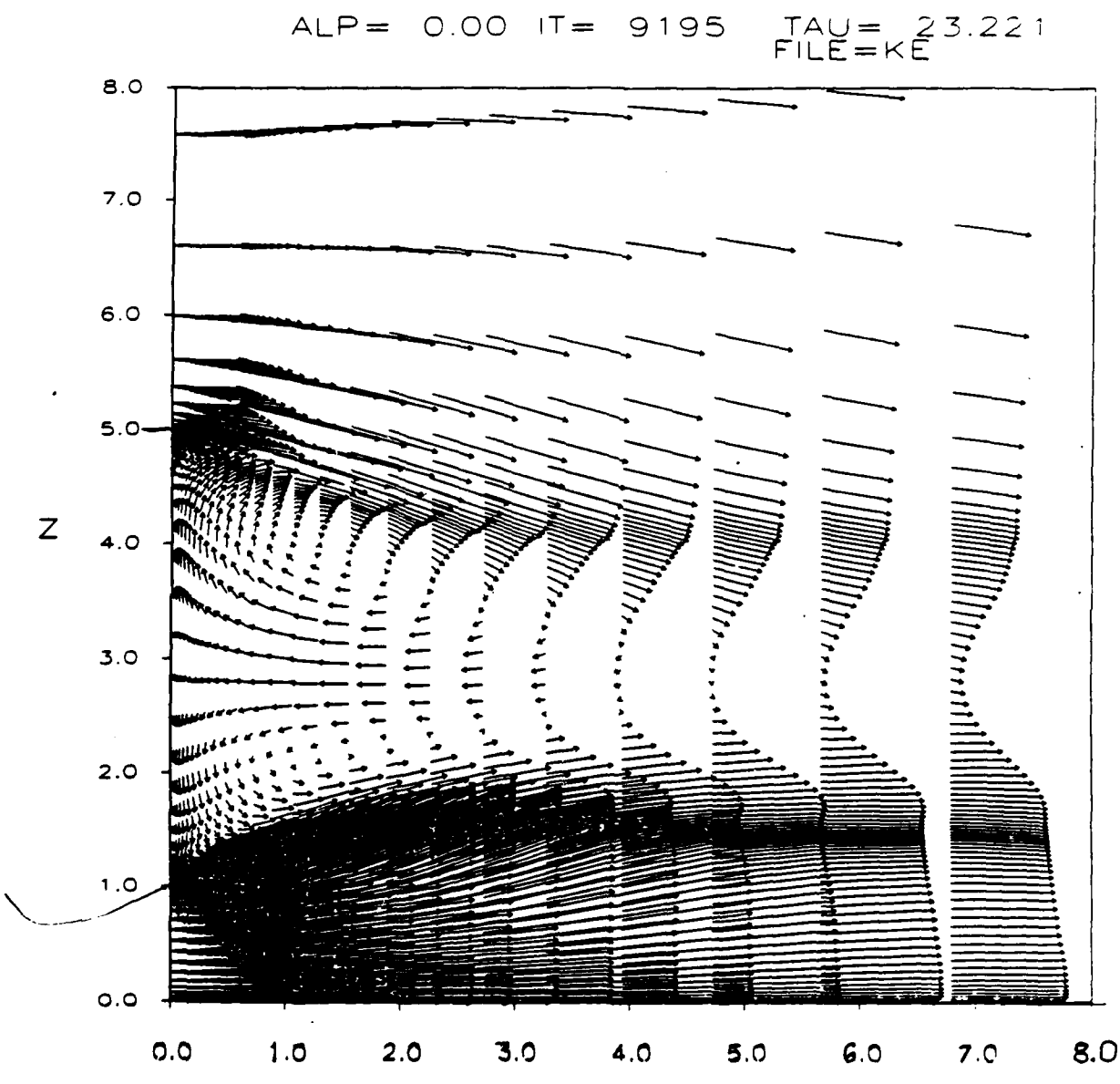

Figure 4.8(a). Velocity vectors in region downstream of base, k-epsilon turbulence model.

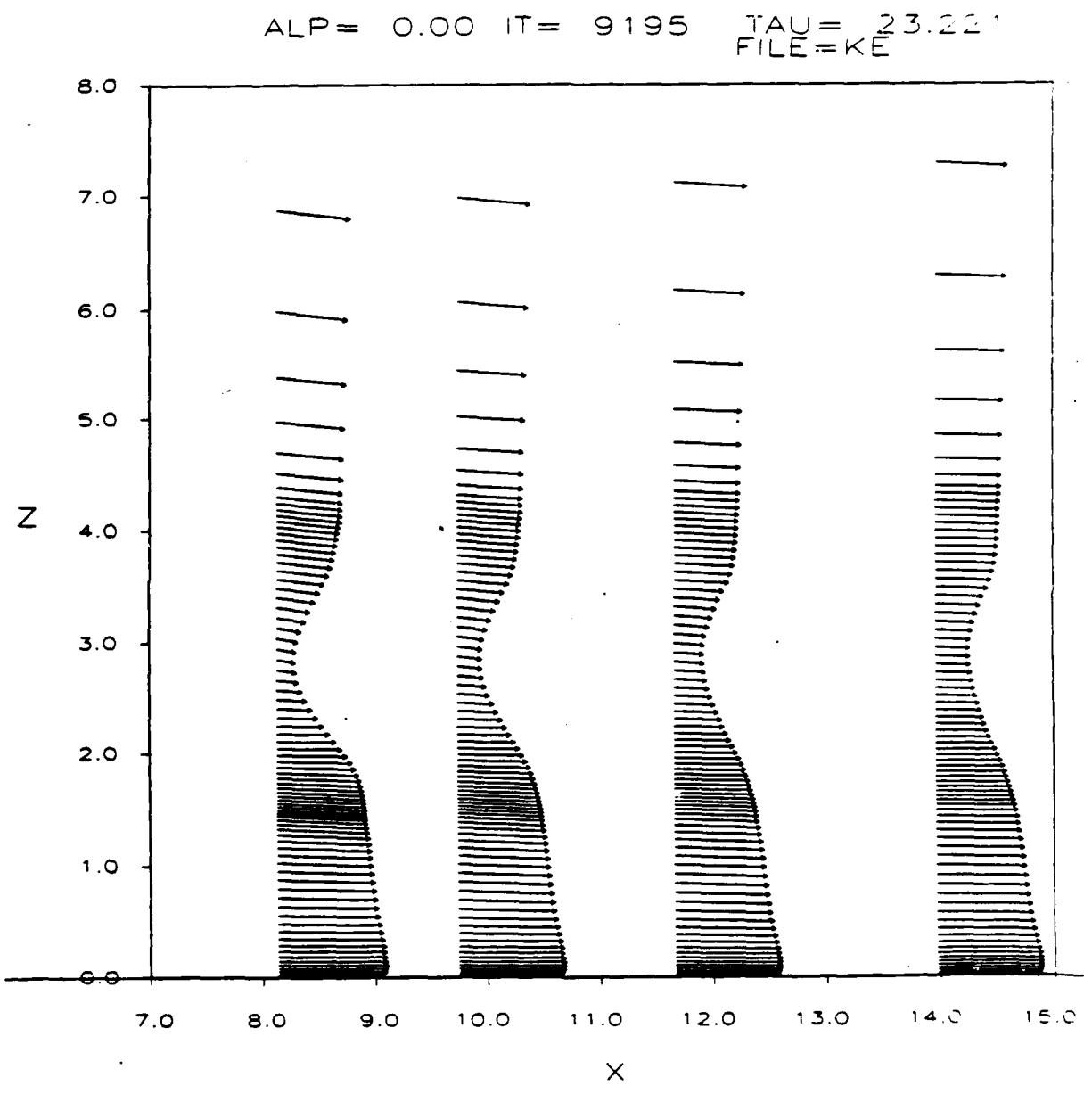

Figure 4.8(b). Velocity vectors in region downstream of base, k-epsilon turbulence model.

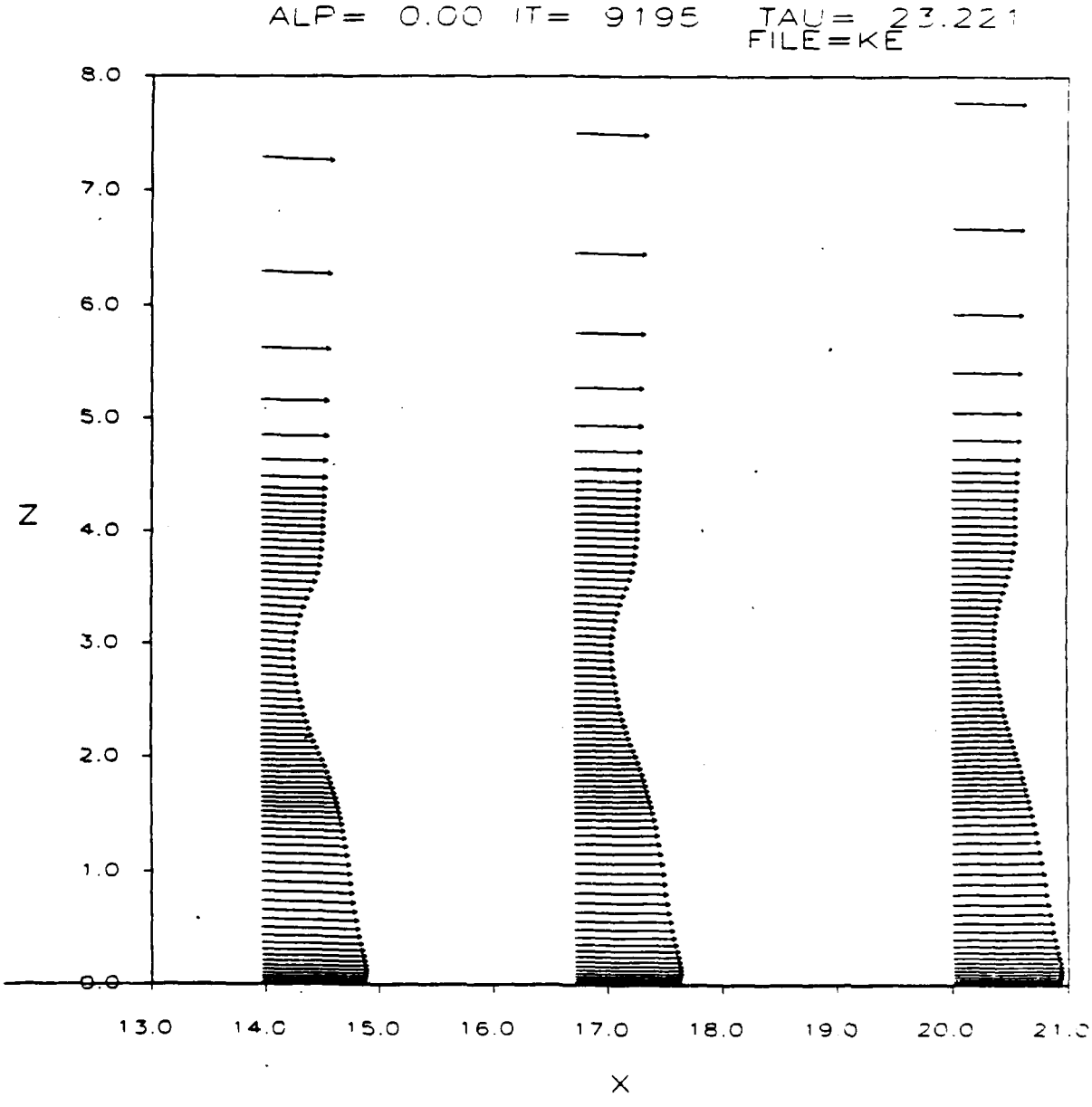

Figure 4.8(c). Velocity vectors in region downstream of base, k-epsilon turbulence model.

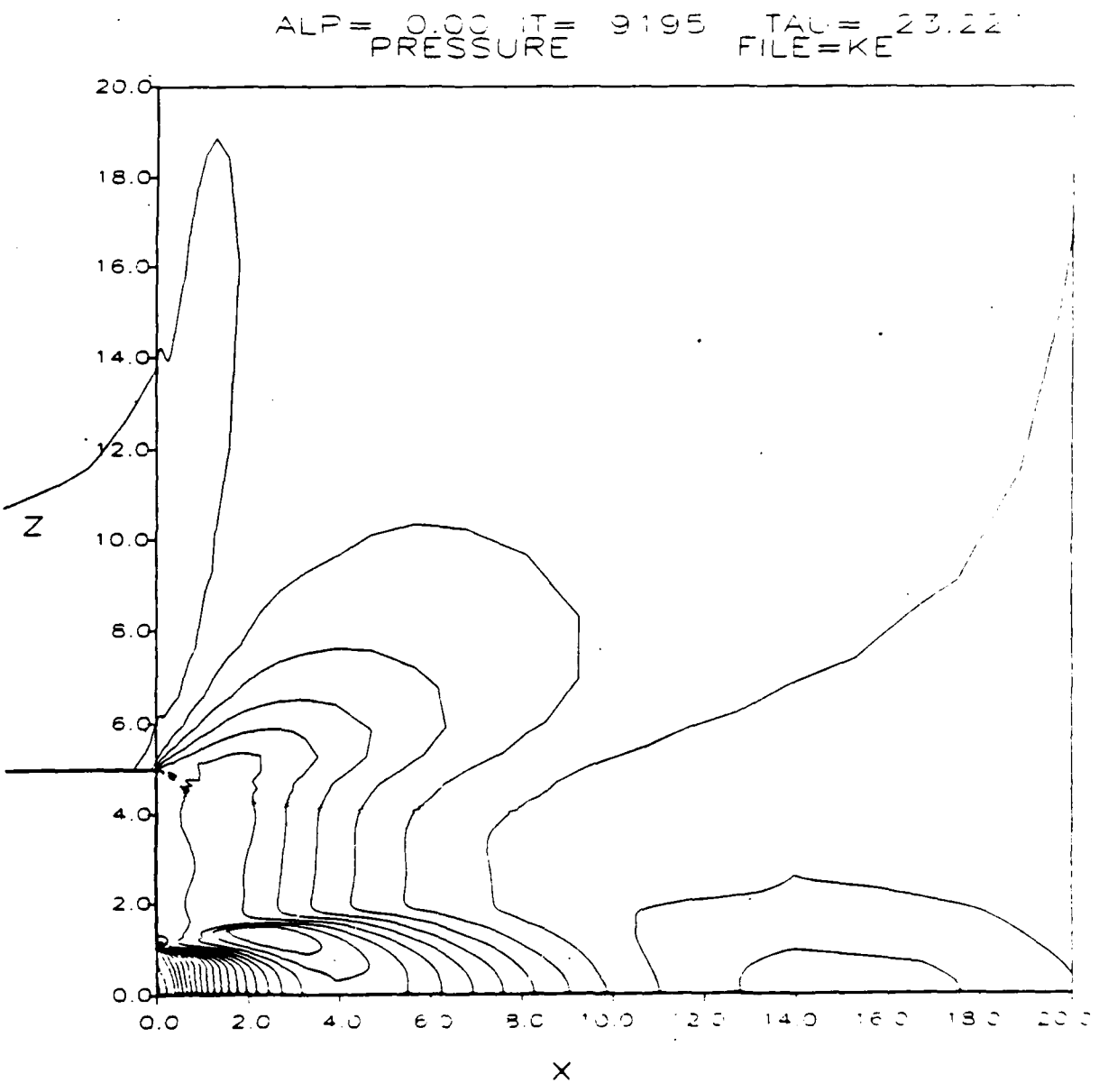

Figure 4.9. Pressure contours in base flow region, k-epsilon turbulence model.

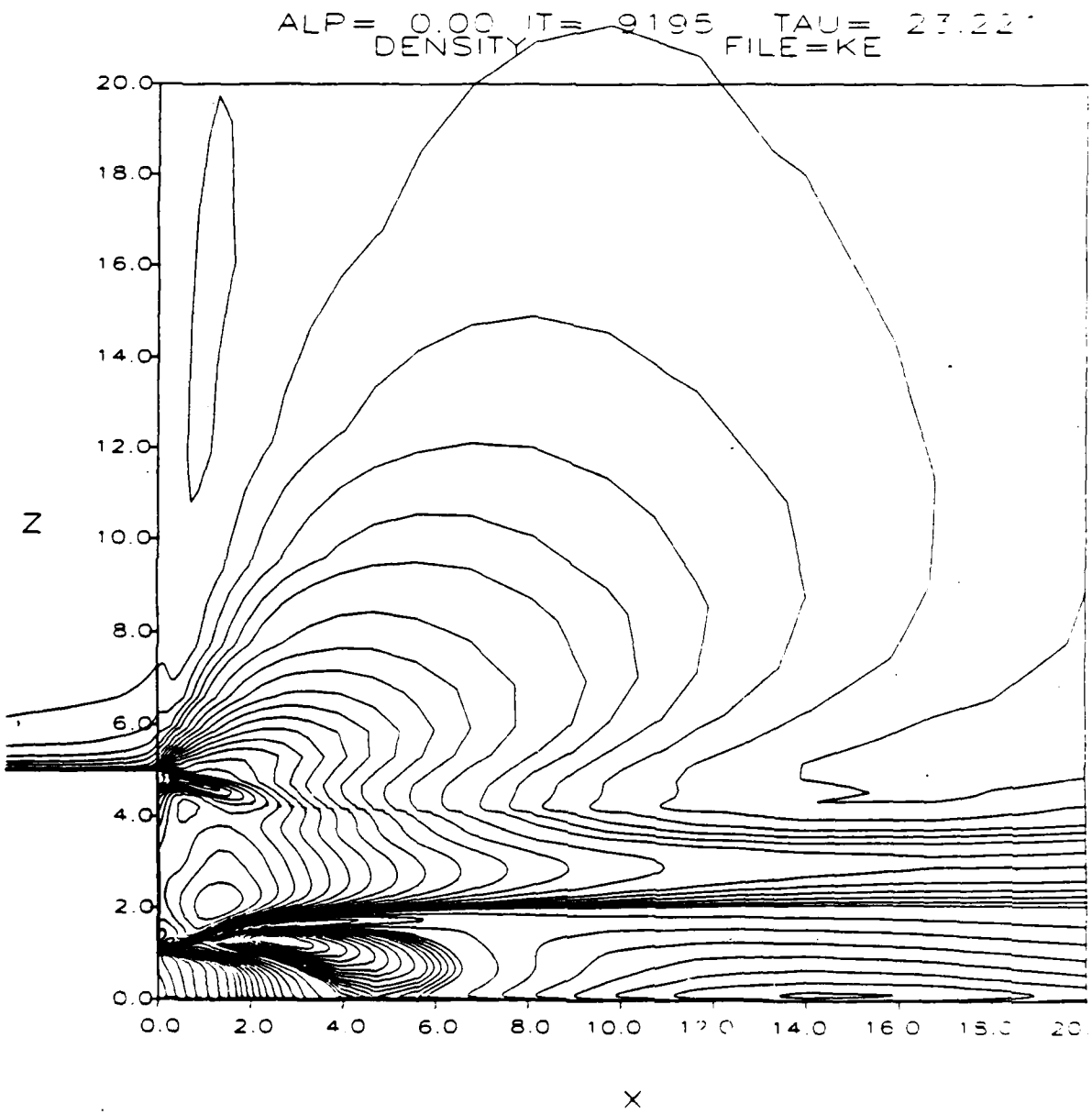

Figure 4.10. Density contours in base flow region, k-epsilon turbulence model.

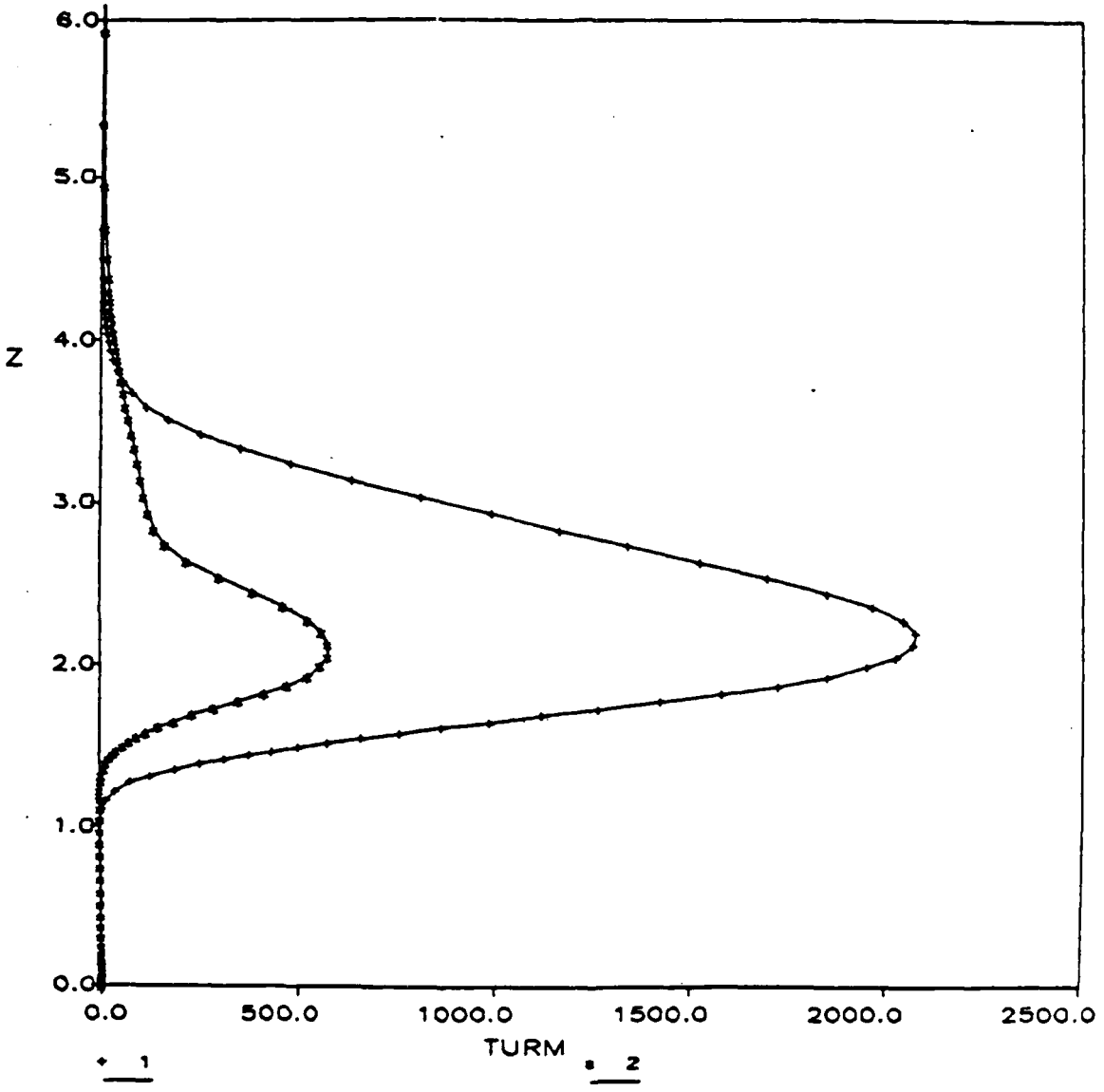

Figure 4.11. Comparison of radial profiles of turbulent eddy viscosity at axial station X=6: (1) k-epsilon model, (2) k-W model.

REFERENCES

Anon., "Analysis of the Axisymmetric Base Pressure and Base Temperature Problem with Supersonic Interacting Freestream-Nozzle Flows based on the Flow Model of Korst, et al.," Parts I-III, MICOM Reports RD-TR-69-12 through RD-TR-69-14, U.S. Army Missile Command, Redstone Arsenal, Ala., 1969.

Arora, R., Kuo, K.K., and Razdan, M.K., "Near-Wall Treatment for Turbulent Boundary Layer Computations," AIAA J., Vol. 20, No. 11, Nov. 1982, pp. 1481-1482.

Baldwin, B.S., and Lomax, H., "Thin Layer Approximation and Algebraic Model for Separated Turbulent Flows," AIAA Paper No. 78-257, 16th Aerospace Sciences Meeting, Huntsville, Ala., Jan. 1978.

Beam, R. and Warming, R.F., "An Implicit Factored Scheme for the Compressible Navier-Stokes Equations," AIAA Journal, Vol. 16, No. 4, April, 1978, pp. 393-402.

Chien, K.Y., "Predictions of Channel Boundary Layer Flows with a Low-Reynolds-Number Turbulence Model," AIAA J., Vol. 20, Jan. 1982, pp. 33-38.

Deiwert, G.S., "A Three-Dimensional Afterbody/Exhaust Plume Navier-Stokes Code," Proceedings, JANNAF 13'th Plume Technology Meeting, Houston, Texas, April, 1982.

Deiwert, G.S., "Numerical Simulation of Three-Dimensional Boattail Afterbody Flowfields," AIAA J., Vol. 19, No. 5, May, 1981, pp.582-588.

Jones, W.P., and Launder, B.E., "The Prediciton of Laminarization with a Two-Equation Model of Turbulence," Int. Jour. of Heat and Mass Transfer, Vol. 15, 1972, pp. 301-314.

Launder, B.E., and Spalding, D.B., "Mathematical Models of Turbulence," Academic Press, London and new York, 1972.

Mace, A.C.H., Markatos, N.C., Spalding, D.B., and Tatchell, D.G., "Computational Analysis of Combustion in Recirculating Flow for Rocket Exhausts in Supersonic Streams," Paper No. AIAA-81-1386, AIAA/SAE/SME Joint Propulsion Conference, Colorado Springs, Colo. July 1981.

Nietubicz, C.J., Pulliam, T.H., and Steger, J.L., "Numerical Solution of the Azimuthal-Invariant Thin-Layer Navier-Stokes Equations," Paper No. 79-0010, AIAA 17th Aerospace Sciences Meeting, New Orleans, La., Jan. 1979.

Pulliam, T.H., and Steger, J.L., "Implicit Finite-Difference Simulations of Three-Dimensional Compressible Flow," AIAA J., Vol. 18, Nol 2, Feb. 1980, pp. 159-167.

Reklis, R.P., and Thomas, P.D., "A Shock-Capturing Algorithm for the Navier-Stokes Equations," AIAA paper 81-1021, Proceedings of the AIAA 5th Computational Fluid Dynamics Conference, Palo Alto, California, June 1981.

Reklis, R.P., Conti, R.J., and Thomas, P.D., "Numerical Simulation of Hypersonic Viscous Flow Over Cones at Very High Incidence," Paper No. AIAA-83-1669, 16th Fluid and Plasmadynamics Conference, Danvers, Mass., July, 1983.

Spalding, D.B., "A Two-Equation Model of Turbulence," VDI Forsch.-Heft [549], 1972, pp. 5-16.

Thomas, P.D., "Boundary Conditions for Implicit Solutions to the Compressible Navier-Stokes Equations on Finite Computational Domains," AIAA Paper 79-1447, Proceedings of the AIAA 4th Computational Fluid Dynamics Conference, Williamsburg, Va., July, 1979.

Thomas, P.D., and Lombard, C.K., "The Geometric Conservation Law and its Application to Fluid Dynamic Computations on Moving Grids," AIAA Journal, Vol. 17, No. 10, Oct. 1979, pp. 1030-1037.

Thomas, P.D., "Numerical Method for Prediction Flow Characteristics and Performance of Nonaxisymmetric Nozzles - Theory," NASA CR-3147, Sept. 1979.

Thomas, P.D., "Numerical Method for Predicting Flow Characteristics and Performance of Nonaxisymmetric Nozzles. Part 2 - Applications," NASA CR-3264, October 1980.

Thomas, P.D., and Neier, K.L., "User's Guide for the NOZL3D and NOZLIC Computer Programs (Core Memory Resident Versions)," NASA Contractor Report LMSC-D767057, October, 1980.

DISTRIBUTION

	No. of Copies
US Army Materiel System Analysis Activity ATTN: AMXSY-MP Aberdeen Proving Ground, MD 21005	1
IIT Research Institute ATTN: GACIAC 10 W. 35th Street Chicago, IL 60616	1
AMSMI-RD, Dr. McCorkle	1
Dr. Rhoades	1
-RD-SS-AT	20
-RD-CS-R	15
-RD-CS-T	1
-GC-IP, Mr. Fred M. Bush	1

END

DATE

FILMED

9-88

DTIC